Redox Biochemistry and Chemistry 5–6 (2023) 100009

Contents lists available at ScienceDirect

Redox Biochemistry and Chemistry

journal homepage: www.journals.elsevier.com/redox-biochemistry-and-chemistry

Electron paramagnetic resonance (EPR) for investigating relevant players of redox reactions: Radicals, metalloproteins and transition metal ions

Ohara Augusto *, Daniela Ramos Truzzi, Edlaine Linares

Departamento de Bioquímica, Instituto de Química, Universidade de São Paulo, São Paulo, Brazil

ARTICLE INFO

Keywords:
EPR
EPR methodologies
Free radicals
Transition metal ions
Metalloproteins
Spin trapping

ABSTRACT

Electron paramagnetic resonance (EPR) spectroscopy is unique in providing robust information about free radicals, transition metal ions and metalloenzymes, which are crucial players in redox processes. EPR had a major role in advancing the redox biology field during the 20th century, but the interest in this methodology considerably decreased in recent years. Here, we discuss potential reasons for this decline as well as potential reasons for maintaining the mind open to the many possibilities brought by EPR and associated methodologies to the redox field. We present the fundamentals of EPR using pictorial images and minimal physicochemical language. We also present EPR derived methodologies developed to detect radical metabolites, that is, direct EPR of solutions (static and continuous-flow), direct EPR of frozen solutions, spin-trapping and spin-scavenging, showing examples and discussing the advantages and drawbacks of each one. Finally, we discuss the EPR spectra of metalloproteins and metal ion complexes of biological interest, which are more complex than those of radical metabolites in solution. In addition to introduce EPR methodologies to those new to the redox field, our goal is to show that these methodologies can contribute to advance the field.

1. Introduction

Redox biology began with the realization that aerobic metabolism produces free radicals that can cause damage to biomolecules, cells and organisms [1–3]. Although it was recognized that nonradical oxidants (2 electron oxidants) are biologically produced, the prominence of radicals (1 electron oxidants) was such that this area of investigation was initially named "free radicals in biology" or subtle variations of it. Not surprisingly, electron paramagnetic resonance (EPR) spectroscopy, the gold standard for detection and characterization of radicals, had an important role in advancing the redox area up to the end of the 20th century.

The 90′s brought the discoveries of the signaling functions of $NO^{\bullet}$ [4,5] and H_2O_2 [6]. These paradigmatic discoveries and the following advances led to the recognition that oxidants and radicals are not always toxic to cells and organisms, but also mediate cellular signaling and regulation. Then, most of the attention of redox biology area diverted from free radicals to nonradical oxidants and from oxidative damage to cellular responses to oxidants, in particular responses to H_2O_2 [7–9].

However, cellular redox signaling and cellular regulation are far from being elucidated and the participation of radicals in these processes cannot be excluded [10]. The signaling function of the radical $NO^{\bullet}$ is undisputable, although its better characterized action mechanism (binding to the heme group of guanylate cyclase and enzyme activation) [11,12] is unrelated to the classical redox signaling mechanism based on the oxidation/reduction of thiol proteins [13].

The evolution of the redox biology area led to an increased interest in techniques sensitive enough to detect oxidants (or their products) in organelles, cells and tissues under pathophysiological and even physiological conditions. This stimulated the development of methodologies based on fluorescence, mass spectrometry and microscopy, taking advantage of the contemporary advances in these techniques. In parallel, the general interest in EPR methodologies considerably declined, despite these methodologies being unique in providing robust information about radicals, transition metal ions and metalloenzymes, all of which are crucial players in redox processes.

The redox mechanisms underlying biological phenomena are complex and multi-faceted and a comprehensive understanding of these mechanisms requires multidisciplinary approaches and a combination of most of the available techniques. Therefore, it is tactical to keep an open mind to the many possibilities that EPR and associated methodologies bring to the redox field. Here, we discuss the fundamentals of EPR using pictorial images and minimal physicochemical language,

* Corresponding author. Departamento de Bioquimica, Instituto de Química, Universidade de São Paulo, Av Lineu Prestes, 748, 05508-000, São Paulo, SP, Brazil.
E-mail address: oharaugusto@gmail.com (O. Augusto).

https://doi.org/10.1016/j.rbc.2023.100009
Received 23 June 2023; Received in revised form 25 July 2023; Accepted 28 July 2023
Available online 29 July 2023

Abbreviations

DBNBS	3,5-dibromo-4-nitrosobenzenosulfonic acid
DMPO	5,5-dimethyl-1-pyrroline-N-oxide
DEPMPO	diethoxyphosphoryl-5-methyl-1-pyrroline N-oxide
MNP	2-methyl-2-nitrosopropane
PBN	N-tert-butyl-α-phenylnitrone
POBN	α-(4-pyridyl-1-oxide)-N-tert-butylnitrone
peroxynitrite	the sum of peroxynitrite anion (ONOO⁻, oxoperoxonitrate (−1)) and peroxynitrous acid (ONOOH, hydrogen oxoperoxonitrate)
tempol	4-hydroxy-2,2,6,6-tetramethyl-1-piperidinyloxy radical

recommending two excellent texts for those who want to delve deeper [14,15]. We also present and discuss the EPR methodologies developed to detect radical metabolites as well as metalloproteins and metal ion complexes of biological interest, providing examples and complementary literature. Our goal is to introduce EPR methodologies to newcomers to the redox field while showing that these methodologies contribute to advance the knowledge on redox mechanisms underlying chemical and biological phenomena.

2. EPR basics

EPR (also called electron spin resonance (ESR)) is a form of magnetic resonance spectroscopy as is the case of nuclear magnetic resonance (NMR). All forms of spectroscopy are based on the absorption of electromagnetic radiation by a molecule resulting in its transition from a ground (lower energy) state to an excited (or higher energy) state (Fig. 1A). For the transition to occur, the radiation frequency must be equal to the energy difference between the ground and excited state, which depend on the intrinsic physicochemical properties of the analyzed molecule(s). The transition energies in UV spectroscopy (ν ~10^{17}-10^{15} Hz) correspond to the strong electrostatic bond energies of the molecule valence electrons. In contrast, the transition energies in magnetic resonance spectroscopy are much smaller because they correspond to the weak interactions of an external magnetic field with either, the electron magnetic moment for EPR spectroscopy (ν~10^{12}–10^{10} Hz) or with the nuclear magnetic moment of nuclei for NMR spectroscopy (ν~10^{6}–10^{9} Hz) [15].

Many nuclei have a magnetic moment (nuclei possessing an odd number of protons or an odd number of protons plus neutrons) justifying the many applications and extensive use of NMR. In contrast, only radicals and transition metal ions with unpaired electrons possesses electron magnetic moment because electrons that occupy the same orbital have opposite spins (Pauli principle), cancelling each other out. Therefore, EPR is specific for radicals and transition metal ions.

In a quantum mechanical description, the magnetic moment of a nucleus or an electron is related to their corresponding spins, which define the orientations they can take relative to an external magnetic field (H). Each of these orientations corresponds to a distinct energy level. Magnetic resonance absorptions correspond to transitions between these energy levels. The electron spin (S) is ½, specifying two orientations relative to the magnetic field: −½ parallel to the magnetic field (low energy) or +½ antiparallel to it (high energy). A pictorial view of a typical experiment EPR experiment is displayed in Fig. 1 B. In the absence of an external magnetic field, the spin population (unpaired electrons) of a solution containing free radicals at room temperature, for instance, is distributed randomly and has the same energy level on average. With the application of the magnetic field of a EPR spectrometer, the spin population can assume one of two orientations relative to the magnetic field, parallel (−½) or antiparallel (+½), but the former is preferred because it has lower energy. The gap of energy between these states varies with the magnetic field strength (Fig. 1B), and the EPR signal is due to the absorption of the energy necessary to promote spins from the lower energy to the higher energy population according to Equation (1):

$$\Delta E = \left(E_{(ms=½)} - E_{(ms=-1/2)}\right) = h\nu = g\beta H \quad (1)$$

where h, Planck's constant; ν, microwave frequency; g, the position in the magnetic field where the resonance occurs (specific for each radical/transition metal ion), β, Bohr magneton (a physical constant for expressing the magnetic moment of an electron); and H, the applied magnetic field.

The g value for a free electron is 2.0023. Most radicals have a g value very close to that of the free electron, but slightly different (±0.2 at most) because in each radical the unpaired electron has a different structural neighborhood. For instance, radicals with extensive spin delocalization, especially on heteroatoms, have higher g values [16]. Metalloproteins and metal ion complexes, however, have g values markedly different from that of the free electron (see *4.*).

Equation (1) permits the calculation of the magnetic field required for an EPR experiment. The microwave frequencies used in commercial instruments are usually 9 GHz (X band) or 35 GHz (Q band), requiring fields of 3.2 kG and 12.5 kG, respectively. The EPR spectrum is usually obtained by increasing the magnetic field while simultaneously submitting the sample to a constant microwave frequency. The absorption of microwave energy is detected but, different from other spectroscopies, the EPR spectrum was initially recorded as the first-derivative of the absorption peak (due to instrumental reasons), and this tradition is usually maintained up to these days (Fig. 1B).

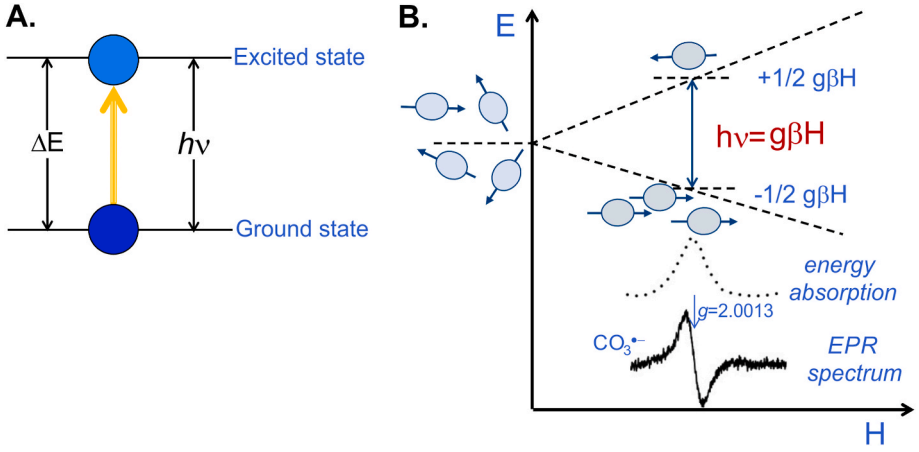

Fig. 1. A. Spectroscopic transition involved in absorption spectroscopy. **B.** Schematic illustration of a typical EPR experiment showing that the EPR signal is due to the absorption of the energy necessary to promote spins from the lower to the higher energy state in the population of unpaired electrons (spins) of a free radical solution submitted to the magnetic field of a EPR spectrometer (see text). All scales in the figure are arbitrary and chosen to illustrate an EPR experiment. The EPR spectrum that illustrates the figure corresponds to that of 2.6 μM carbonate radical ($CO_3^{\bullet-}$) recorded ~1 ms after 1:1 mixing of 4 mM peroxynitrite at pH 12 with 0.1 M bicarbonate/CO_2 in 0.4 M phosphate at pH 6.9 using the continuous flow technique modified with permission from Ref. [18].

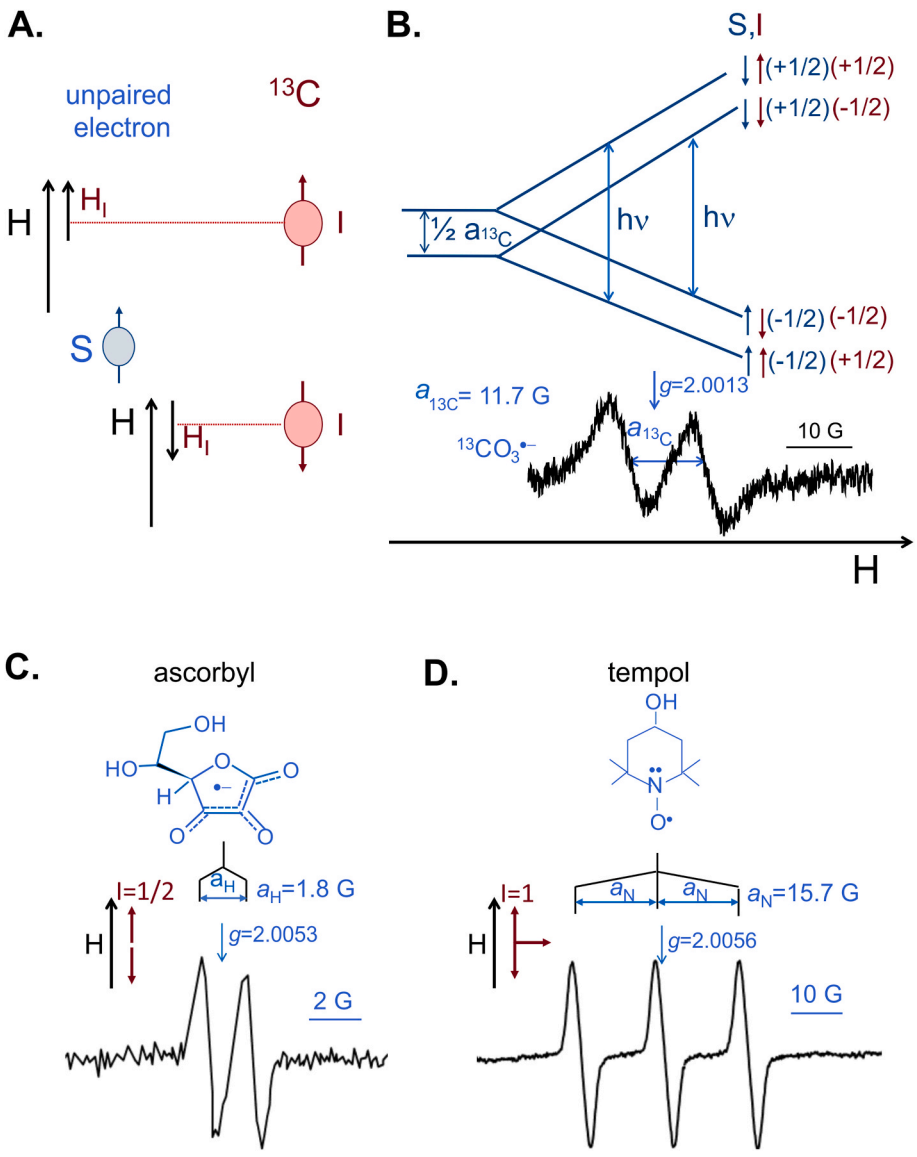

Fig. 2. A. Schematic representation of the hyperfine interaction of an electron spin (S) interacting with the different orientations (parallel or antiparallel) of the nuclear spin of a nucleus of ^{13}C (I = ½). The electron spin (S) experiences a magnetic field arising from the nuclear magnetic moment of ^{13}C (H_I) as well as the EPR spectrometer field (H) (see text). **B.** Shows the effects of the same hyperfine interaction (electron spin with a single nucleus of ^{13}C) on the energy levels of the labeled carbonate radical ($^{13}CO_3^{\bullet-}$) under an external magnetic field at constant frequency ($h\nu$). Under these conditions, two resonance conditions are possible, since the orientation of the nuclear spin does not change during an EPR experiment ($\Delta I_z = 0$). The arrows represent the direction of the magnetic moments. All scales in **A.** and **B.** are arbitrary and chosen to illustrate a hyperfine interaction. The illustrative EPR spectrum of $^{13}CO_3^{\bullet-}$ was modified from Ref. [18] with permission. **C.** EPR spectrum of the ascorbyl radical taken from human plasma treated with peroxynitrite. The figure schematically shows the interaction of the nuclear spin (I) with the instrument magnetic field (H) as arrows and the interaction of the electron and nuclear (H, I = ½) magnetic moments as a fork (for better understanding the number of lines in the EPR spectrum); the *g* and hyperfine constant (a_H) values of the ascorbyl radical are also shown. **D.** The same as **C.** for tempol (50 μM) in phosphate buffer, pH 7.4. The spectra are from the personal archive of the authors.

Table 1
The nuclear magnetic spin (I) of nuclei abundant in biomolecules and some of their isotopes.

Nucleus	Abundance %	Nuclear spin (I)	Number of lines (2I +1)
^{1}H	99.99	1/2	2
^{14}N	99.63	1	3
^{15}N	0.37	1/2	2
^{12}C	98.93	0	0
^{13}C	1.07	1/2	2
^{16}O	99.76	0	0
^{17}O	0.04	5/2	6
^{31}P	100	1/2	2

The EPR spectrum of a paramagnetic molecule under determined experimental and instrumental conditions provides its *g* value (Eq. (1)), as well as its concentration. Indeed, the level of absorbed energy is proportional to the unpaired electron concentration. This concentration can be obtained by the double integral of the EPR signal and comparison with known concentrations of a standard radical or transition metal ion spectrum scanned under the same experimental and instrumental settings. For instance, the EPR spectrum that illustrates Fig. 1B corresponds to that of 2.6 μM carbonate radical ($CO_3^{\bullet-}$) (g = 2.0113) recorded approximately 1 ms after mixing (1:1 v/v) 4 mM peroxynitrite at pH 12 with 0.1 M bicarbonate/CO_2 in 0.4 M phosphate at pH 6.9 using the continuous flow technique (see *3.2.*). The concentration of $CO_3^{\bullet-}$ was determined by normalizing its doubly integrated EPR signal to that of 2 μM of the stable radical tempol (4-hydroxy-2,2,6,6-tetramethyl-1-piperidinyloxy radical) scanned under the same conditions [17,18].

Not all radicals have a monotonous one-line EPR spectrum (one resonance condition) because the free electron interacts with neighboring nuclei that have nuclear spin magnetic moment (I) leading to the splitting of the energy levels into amounts called hyperfine splitting constant (*a*) (Fig. 2). Among the nuclei that are abundant in biomolecules and have nuclear spin different from zero are ^{1}H (abundance 99.99% (I = ½) and ^{14}N (I = 1) (abundance 99.63%) (Table 1). The most abundant isotopes of carbon (^{12}C) and oxygen (^{16}O) are diamagnetic (I = 0), explaining the one-line spectrum of the $CO_3^{\bullet-}$ (Fig. 1B). To unequivocally prove that the radical detected by rapid continuous flow EPR mixtures of peroxynitrite and bicarbonate/CO_2 was the $CO_3^{\bullet-}$, the reagent was substituted by the ^{13}C-labeled one ($H^{13}CO_3^-/^{13}CO_2$). In this case, a two-line EPR spectrum was detected (with half peak height) as expected for a $^{13}CO_3^{\bullet-}$ radical [17,18]. This is because in $^{13}CO_3^{\bullet-}$ the unpaired electron (S) experiences a magnetic field arising from the ^{13}C

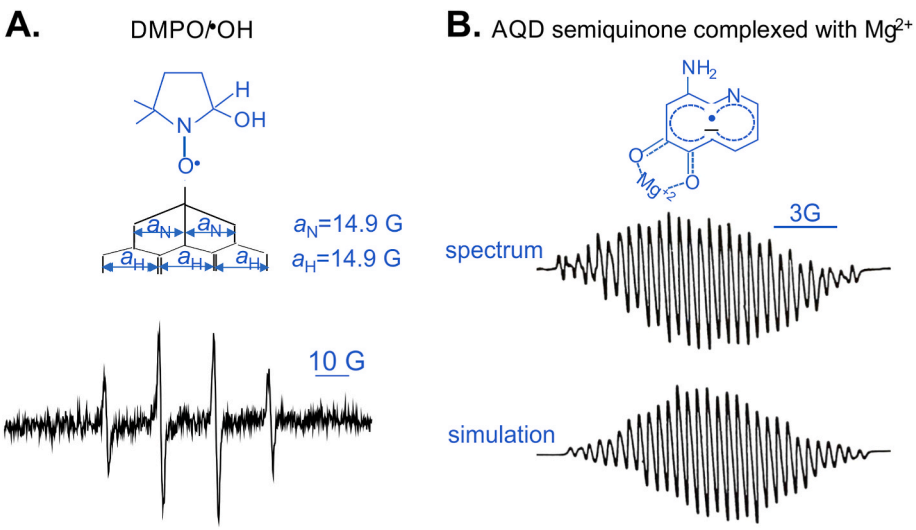

Fig. 3. A. EPR spectrum of the DMPO/•OH radical adduct in phosphate buffer, pH 7.4 obtained from spin trapping experiments with DMPO in macrophages pre-treated with buthionine sulfoximine (BSO) and subsequently with peroxynitrite [83]. **B.** EPR spectrum of 5,6-dihydroxy-8-aminoquinoline (AQD) semiquinone (a metabolite of the antimalarial primaquine) complexed with Mg^{+2} ions (top spectrum) and its computer simulation (bottom spectrum) [20]. The simulation was performed in a small computer by considering the following hyperfine constants: $a_N = 1.87$ G, $a_N = 0.134$ G, $a_H = 2.34$ G (2H), $a_H = 0.92$ G, $a_H = 0.51$ G (2H), $a_H = 0.29$ G [20].

magnetic moment (H_I) as well as the applied magnetic field (H) (Fig. 2A). The direction of the field arising from ^{13}C (I = ½) can either oppose or reinforce the spectrometer magnetic field. Consequently, the unpaired electron effectively experiences either of two different magnetic fields (H – H_I) or (H + H_I) and the EPR signal splits in two. Fig. 2B shows the effect of the hyperfine interaction on the energy levels of the $^{13}CO_3^{\bullet -}$ unpaired electron, noting that under an EPR experiment electron spin transitions occur (−½ to +½; $\Delta S_z = 1$) but nuclear spin transitions do not ($\Delta I_z = 0$). At constant frequency ($h\upsilon$) two resonance conditions are possible, demonstrating that a previous single transition ($CO_3^{\bullet -}$) splits into a doublet or a two-line EPR signal due to the hyperfine interaction between the free electron and ^{13}C in the case of the $^{13}CO_3^{\bullet -}$ (Fig. 2B).

Likewise, the ascorbyl radical (produced from the one-electron oxidation of the vitamin C, an important plasma and cellular antioxidant) displays a two-line EPR spectrum because the free electron interacts more strongly with the H atom (I = ½) attached directly to the ring than with the side chain H atoms (Fig. 2C). Tempol, on the other hand, has a three-line EPR spectrum because the free electron interacts with the N atom (I = 1), the nuclear spin of which may not influence (perpendicular orientation), reinforce (parallel orientation) or oppose (antiparallel orientation) the instrument magnetic field (Fig. 2D). In addition to the spectrum, Fig. 2C and D schematically show the interaction of the nuclear spin with the instrument magnetic field, the fork scheme (which shows the free electron absorption splitting by interaction with each of close nucleus with magnetic moment, facilitating EPR spectrum attribution); these figures also display the *g* and hyperfine constant values (*a*) of each specific radical.

In summary, the number of lines observed in an EPR spectrum is given by Equation (2):

$$\text{Number of lines} = 2nI + 1 \quad (2)$$

where n is the number of equivalent nuclei with spin I. In all the radicals displayed in Fig. 2, the unpaired electron interacts with one nucleus having a magnetic moment (n = 1) and the number of lines depends on its corresponding spin (I). In radicals in which the unpaired electron interacts with inequivalent nuclei (different magnetic moment or chemically inequivalent), the total number of lines is multiplied. In some cases, these lines occur at identical field values resulting in line superposition. This is exemplified in the case of DMPO-hydroxyl radical adduct (DMPO/•OH) [19], in which the unpaired electron interacts with one N (3 lines) and one H (2 lines), but the hyperfine splitting constants of the two atoms coincide, resulting in a four-line spectrum with relative heights of 1:2:2:1 (Fig. 3A), instead of a six-line spectrum (3 × 2) of the same height.

Therefore, to identify a radical by its EPR spectrum, one considers the number of lines and the relative height of these lines, which reveal the nuclei with magnetic moment interacting with the unpaired electron. In the case of complex EPR spectra, simulation programs help interpreting them. For instance, autoxidation of 5,6-dihydroxy-8-aminoquinoline (AQD), a metabolite of the antimalarial primaquine, led to detection of a well-resolved and complex EPR spectrum in the presence of Mg^{+2} ions (Fig. 3B). The spectrum was assigned to the semiquinone of the AQD complexed with Mg^{+2} based on a reasonable computer simulation of the spectrum (Fig. 3B) and additional data showing redox cycling of the corresponding quinone [20]. The hyperfine constant values extracted by the correlation method [21] are shown in the legend of Fig. 3, but they were not assigned to specific magnetic nuclei because this would require synthesis of the compound with isotopic substitutions (^{15}N and ^{2}H) [22].

Up to this point, we emphasized that EPR reveals the presence of radicals and provides information about their chemical structure and concentration. However, EPR spectra are very sensitive to the physical properties of radical microenvironment, such as viscosity, polarity and presence of other paramagnetic species [14,15]. A few of these aspects will be presented below, but not in depth because they are beyond the scope of this review focused on the detection of biologically relevant radicals and metal ion complexes.

3. EPR methodologies to investigate biologically relevant radicals

It would be easy to detect and characterize radicals of biological interest by EPR if they were all as stable (long-lived) as the ascorbyl radical (a natural product) (Fig. 2C) and tempol (a synthetic compound) (Fig. 2D) that are stabilized by electron delocalization. The vast majority of radicals of biological interest has extremely short half-life in aqueous solutions at room temperature and even shorter in crowded physiological environments. Not surprisingly, the EPR spectra shown for the biologically relevant radicals $CO_3^{\bullet -}$ (Figs. 1 and 2A), $HO^{\bullet}$ (DMPO/•OH) (Fig. 3A) and AQD semiquinone (Fig. 3B) were obtained using additional methodologies associated with EPR. The estimated half-life of $HO^{\bullet}$ and $CO_3^{\bullet -}$ in physiological conditions are 1×10^{-9} s [23,24] and around 1×10^{-6} s [25], respectively. Although AQD semiquinone (Fig. 3B) is stabilized by electron delocalization, its half-life was not much longer than 30 s because it was impossible to acquire its well-resolved EPR spectrum in the absence of Mg^{2+} ions [20]. Additionally, biological systems generate radicals at relatively low rates as compared with chemical,

Table 2
Summary of EPR and associated methodologies and corresponding advantages and drawbacks.

Method	Advantages	Drawbacks
Direct EPR (solutions)		
a. static	provides radical structure requires small samples	applicable to long-lived $R^{\bullet}$[1] ($t_{1/2} \geq 30$ s)
b. continuous flow	applicable to short lived radicals ($t_{1/2} \geq 10^{-6}$ s)	requires large samples; does not detect $O_2^{\bullet-}$, $HO^{\bullet}$ and $RS^{\bullet}$
Direct EPR (frozen)	applicable to short lived $R^{\bullet}$; requires small samples. provides structural hints for metal-complexes such as those of $NO^{\bullet}$	quite limited use for organic radicals due to anisotropy
EPR spin trapping	wide application (test tubes, cells and animals); requires small samples; detects $O_2^{\bullet-}$; $HO^{\bullet}$; $RS^{\bullet}$; detects low and high MW[1] $R^{\bullet}$; can be complemented by other techniques (MS[1], MRI[1], immunodetection, isotopic labeling)	indirect method; structural information may be limited
Spin scavenging	wide application; requiressmall samples	not specific for radicals; no structural information

[1]Abbreviations $R^{\bullet}$, generic radical MW; molecular weight; MS, mass spectrometry; MRI molecular resonance imaging.

radiolytic and photolytic processes. Since most radical metabolites are produced at low rates and rapidly react with biotargets, they do not reach steady-state concentrations greater than the detection limit of the EPR instrument, usually between 0.01 and 1 μM, depending on the specific radical. The number of lines of the radical spectrum is particularly relevant for its detection because each hyperfine splitting divides signal intensity. For instance, the many lines of the AQD semiquinone spectrum indicate that a high steady-state concentration of it is necessary for the acquisition of a well-resolved EPR spectrum (Fig. 3B). Therefore, complexation with Mg^{2+} ions was employed to stabilize the semiquinone, because previous studies had shown that ortho-semiquinones are stabilized by complexation with Mg^{2+} or Zn^{+2} ions [26,27].

In fact, different EPR derived methodologies were developed to increase the steady-state concentration of biologically relevant radicals to permit overcoming the detection limit of the EPR instrument. The most common methodologies will be discussed below and are summarized in Table 2, together with their specific advantages and drawbacks. The

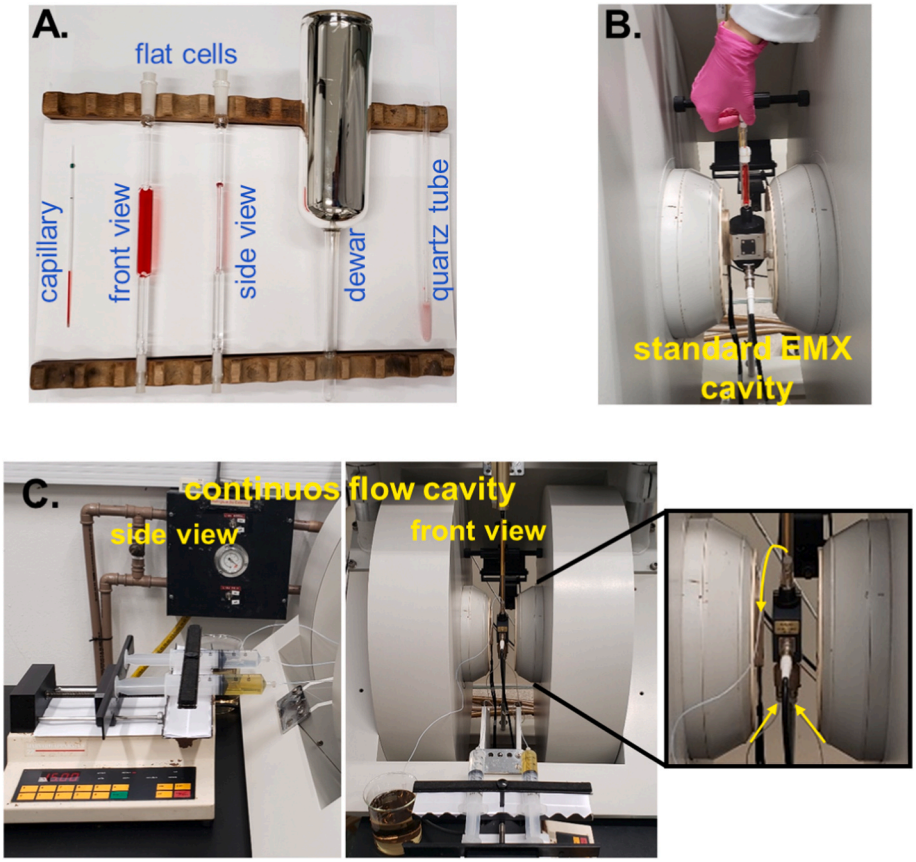

Fig. 4. A. Photo showing the sample containers for EPR experiments as specified. **B.** Photo of a sample in a flat cell being introduced in a standard cavity of a EMX instrument from Bruker. **C.** Photo of the settings for a continuous flow EPR experiment using a Bruker ER mixing resonator (4117 D-MTV). All the photos are from the personal archive of the authors.

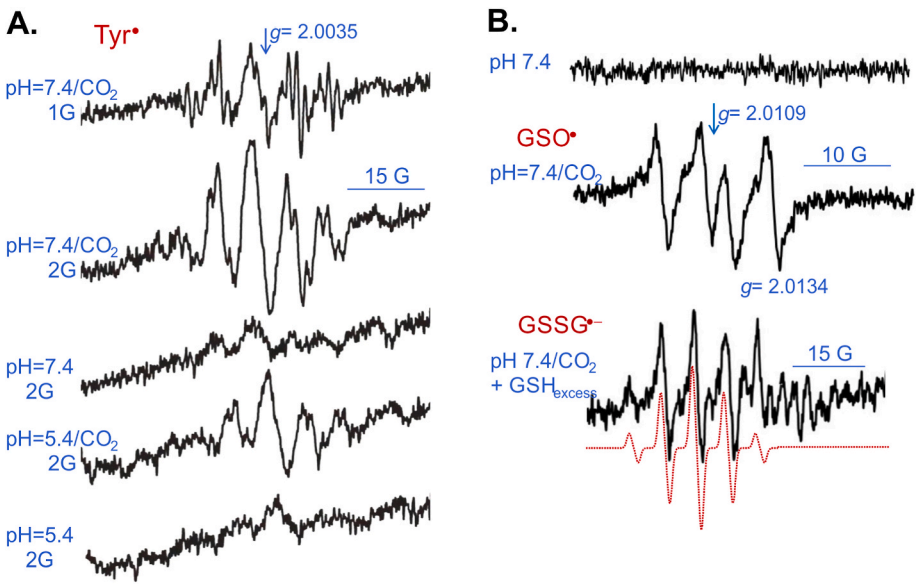

Fig. 5. A. EPR continuous flow spectra of the tyrosyl radical produced from mixing 2 mM peroxynitrite and 3.7 mM tyrosine in the presence or absence of CO_2 in 0.3 M phosphate buffer at the specified conditions. The flow rate was 4 ml/min. Modified from Ref. [51] with permission. **B.** EPR continuous flow spectra of GSH-derived radicals produced from mixing 5 mM peroxynitrite with equimolar or excess GSH in the presence or absence of CO_2 as specified [52]. The flow rate was of 20 ml/min. The spectrum in red is the computer simulation of the $GSSG^{\bullet-}$. (For interpretation of the references to color in this figure legend, the reader is referred to the Web version of this article.)

applicability of each EPR derived methodologies has to be evaluated on a case-by-case basis.

3.1. Direct EPR of samples in solution: static measurements

Direct and static EPR refers to the situation in which the sample is introduced in the cavity of the EPR instrument and spectra scanned at different times or not. Enzymatic and chemical reactions may be started just before introduction of the sample into the cell and the instrument cavity (Fig. 4A and B). The instrument can then provide the EPR spectrum of the steady-state concentration of the produced radical at different times. Sampling time can be reduced by aspirating the sample to the flat cell already in the cavity or by commercial rapid samplers (stopped-flow) [28,29].

The sample volume is small (20–200 μL) in the case of biological samples at room or physiological temperatures because water is extremely lossy at microwave frequencies. Therefore, capillaries are used or flat cells, in the case of volumes higher than 30 μL (Fig. 4A). In the case of rapid samplers, higher volumes are used to fill the connections from sampling to cells. Since optical dispersion is not a limitation to achieve an optimal signal to noise ratio, packed cells or high protein concentration of organelles or purified proteins can be used. These high concentrations may increase the rate of radical formation and, thus the steady-state radical concentration, facilitating its detection. The use of small aqueous samples can be advantageous for precious biological samples.

As previously mentioned, the major problem is that only a few biologically relevant radicals are long-lived enough to be detectable by steady-state static EPR at room temperature. Those that are detectable are stabilized by electron delocalization, and include the one-electron oxidation product of two important natural antioxidants, the ascorbyl radical (see above) (Fig. 2C) and the α-tocopheroxyl radical generated from α-tocopherol (a component of vitamin E).

Phenolic antioxidants derived from plants (flavonoids, hydroxycoumarins, hydroxyantraquinone, etc.) and synthetic ones suffer one-electron oxidation to semiquinones that, depending on structural features, are detectable by direct and static EPR. In some cases, detection requires rapid sampling, stabilization by complexation with metal ions (Zn^{2+}/Mg^{2+}), pH change or DMSO addition [30,31].

Also detectable by static direct EPR are radicals derived from metabolism of many xenobiotics other than phenolic antioxidants, including some medicines. These metabolically produced radicals have been implicated in the toxic and/or therapeutic effect of the xenobiotic, depending on the specific compound. Some of the produced radicals are aromatic radical cations or anions that decay with rate constants on the order of 10^5 M^{-1} s^{-1} and are pH-dependent. Radical cations, such as benzidine cation radical, are more stable at acidic pH values whereas anion radicals, such as antiparasitic nitro-compounds, are more stable at basic pH value [32,33]. Therefore, selecting the pH facilitates detection of these radicals by direct static EPR. Complexation with metal ions (Zn^{2+}/Mg^{2+}) (Fig. 3C) and rapid sampling may also be useful. It also should be noted that many anion radicals react with oxygen to produce $O_2^{\bullet-}$. Consequently, anaerobic conditions may be required to achieve steady-state concentrations above the detection limit of the EPR instrument [28].

Protein-tyrosine residues are frequently oxidized by one-electron mechanisms to produce protein-bound tyrosyl radicals (P-$Tyr^{\bullet}$). Some of these radicals participate in the catalytic mechanism of enzymes while others are formed transiently during enzyme turnover or inhibition. Additionally, uncontrolled formation of protein-$Tyr^{\bullet}$ is increasingly seen as playing a role in the etiology of a range of diseases [34]. Protein-$Tyr^{\bullet}$ located at sterically constrained environments may survive long enough to be detectable by direct EPR at room temperature [35,36]. Nevertheless, well-resolved EPR of protein-$Tyr^{\bullet}$ usually requires rapid sampling or stopped-flow [29], low temperature EPR [37] or spin trapping (see *3.3. and 3.4.*).

We should also mention synthetic cyclic nitroxides, which are easily detectable by direct EPR because they are quite stable radicals due to the three-electron bond between N and O atoms, and are even more stable if α-substituents (such as methyl groups) preclude radical-radical dismutation (Fig. 2C). Hindered nitroxides have long been employed as spin probes (spin labels) in biophysical studies because of their stability and paramagnetic nature [38–40]. More recently, cyclic nitroxides started receiving attention as potential therapeutic agents because of their pronounced antioxidant and anti-inflammatory properties and their low toxicity in animal models of diseases [41–43].

3.2. Direct EPR of samples in solution: continuous flow measurements

The continuous flow EPR methodology permits to detect extremely short-lived radicals (second order decay near the diffusion-controlled limit) by drastically reducing the time between radical formation and detection [44]. The major limitation to apply this methodology to enzymatic reactions is the requirement for incredibly high flows rates

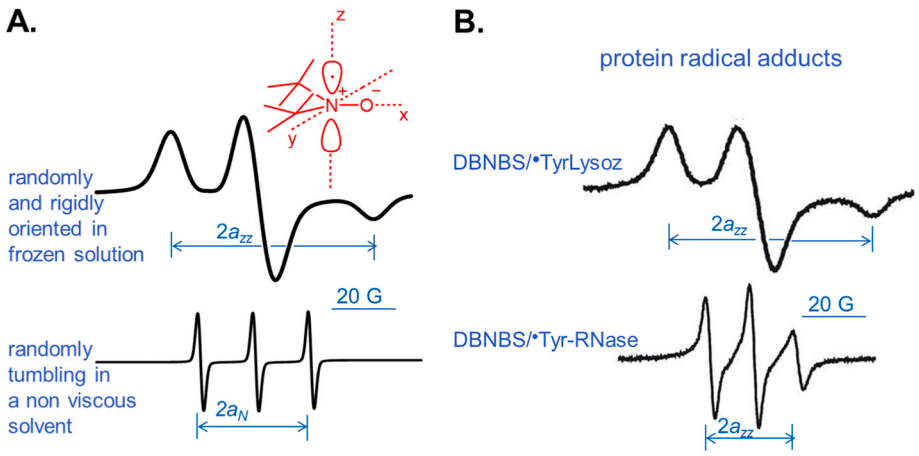

Fig. 6. A. EPR spectra of di-*t*-butyl nitroxide randomly and rigidly oriented in a frozen solution (top spectrum) and EPR spectrum of di-*t*-butyl nitroxide in aqueous solution pH 7.0 (bottom spectrum). The spectra are simulations created with the software WinEPR SimFonia (Bruker) using *g* and hyperfine constant values from the cited refs. [15,61] **B.** EPR spectra of DBNBS protein radical adducts obtained from the oxidation of lysozyme (Lysoz) (top spectrum) or ribonuclease (Rnase) (bottom spectrum) promoted by myeloperoxidase. The incubations contained myeloperoxidase, 10 (U/ml), H_2O_2 (1 mM) and NO_2^- (1 mM), DBNBS (10 mM) and lysozyme (0.35 mM) or ribonuclease (0.35 mM) in acetate buffer, pH 5.4; the spectra were scanned after 30 min of incubation at 37 °C. Modified from Ref. [81] with permission.

(several ml/s depending on the instrumental settings) [45] and high concentrations of enzymes with fast turnovers to attain radical concentrations above the limit of the EPR instrument. Even with the flow in the range of tens ml/min, it is usually too expensive (for commercial enzymes) or too labor intensive (for expressed enzymes) to apply this methodology (Fig. 4C). Not surprisingly, there are few examples of rapid-flow EPR in the study of enzymatic reactions [44,46,47].

The above limitation does not preclude the use of the methodology to investigate processes of biological significance involving chemical systems [45]. Indeed, in a time when the formation of radicals from peroxynitrite was controversial [48], rapid flow EPR was crucial to demonstrate that this oxidant reacts with CO_2 to produce the $CO_3^{\bullet-}$ in considerable yields (approximately 35%) in parallel with $NO_2^{\bullet}$ [17,18]. Peroxynitrite is easily synthesized from inexpensive reagents [49,50]. Therefore, it was possible to employ the high flux rates (14–30 ml/min) required to detect the EPR spectra of $CO_3^{\bullet-}$ (one line) and of $^{13}CO_3^{\bullet-}$ (two lines) (Fig. 1B and 2A, respectively) using a Bruker ER mixing resonator (4117 D-MTV) (Fig. 4C). Soon afterwards, we detected a well-resolved EPR spectrum of the Tyr$^{\bullet}$ in incubations of Tyr (the amino acid tyrosine) in the presence of peroxynitrite/CO_2 at pH 7.4 (Fig. 5A, top spectrum) [51]. In the absence of CO_2 or at pH 5.4 the signal intensities were much lower, requiring a decrease in the spectrum resolution (by using a higher modulation amplitude (2G)) to permit a better comparison of Tyr$^{\bullet}$ yields at different conditions. The experiments using 2 G modulation amplitude (Fig. 5A, 2nd spectrum to bottom spectrum) showed that in the presence of CO_2, the yield of the Tyr$^{\bullet}$ at pH 7.4 was twice that obtained at pH 5.4. Together with calculations, stable product analysis and spin-trapping experiments (see *3.4.*), the results shown in Fig. 5A contributed to demonstrate that protein-tyrosine nitration occurs by a radical mechanism [51]. Likewise, investigating the oxidation of the important intracellular antioxidant GSH (glutathione) by peroxynitrite in the presence and absence of CO_2 and at pHs 7.4 and 5.4, we detected the corresponding sulfinyl radicals (GSO$^{\bullet}$) using equimolar concentrations of thiols and peroxynitrite/CO_2 (Fig. 5B). Using GSH concentration five times higher than that of peroxynitrite, the corresponding disulfide anion radical (GSSG$^{\bullet-}$) was detected (Fig. 5B, bottom spectrum). The oxidation of the amino acid Cys by peroxynitrite/CO_2 provided similar results, with the detection of the corresponding CysSO$^{\bullet}$ and CysS-SCys$^{\bullet-}$ radicals. Taken together with several other experiments, these EPR results demonstrated that at neutral pHs, CO_2 diverts peroxynitrite-mediated oxidation of thiols from two-to one-electron mechanism [52].

Another interesting example of the application of continuous flow EPR was the elucidation of the mechanism responsible for the synergistic protection of low density lipoprotein (LDL) against oxidation by three antioxidants (*α*-tocopherol, caffeic acid, and ascorbate) [53]. The authors examined redox cycling among the three antioxidants by EPR. In the case of *α*-tocopherol and ascorbate, static EPR was used since their corresponding radicals are long lived (see *3.1*). Redox cycling of caffeic acid, however, required continuous flow EPR due to the short half-life of caffeic acid semiquinone. Taken into consideration the obtained results and the physicochemical properties of the three antioxidants, the authors concluded that the synergistic protection against LDL oxidation was due to sequential transfer of the unpaired electron from alfa-tocopheroxyl radical in the lipid phase to caffeic acid at aqueous: lipid interface and the final reduction of caffeic semiquinone radical by ascorbate with formation of ascorbyl radical in the aqueous phase [53].

Despite the utility of continuous flow direct EPR to investigate processes of biological significance, an important drawback is the impossibility of detecting biologically relevant radicals, such as $O_2^{\bullet-}$, HO$^{\bullet}$ and RS$^{\bullet}$ (thiyl)) radicals in aqueous solution at room temperature due to the characteristics of these radicals (short lifetime and broad linewidths) [54,55]. In the case of GSH and Cys oxidation by peroxynitrite/CO_2 (Fig. 5B), it was demonstrated that the corresponding RS$^{\bullet}$ were the precursors of the RSO$^{\bullet}$ and RSSR$^{\bullet-}$ radicals by EPR spin trapping experiments [52]. This technique also allows the detection of $O_2^{\bullet-}$ and HO$^{\bullet}$ (see *3.4.*).

3.3. Direct EPR: frozen samples

The initial phase of reactions can be analyzed if the reaction is stopped by rapid freezing and the EPR spectra scanned. The method was developed by Bray and applied to the detection of $O_2^{\bullet-}$ during xanthine oxidase catalysis [56,57].

The trapping of a radical in a solid matrix at low temperature precludes its decay reactions, increasing radical life-time. Sample tissues can also be investigated by freeze clamping the tissues with tongs cooled in liquid nitrogen or, in the case of liquid biological samples, by rapidly freezing them in liquid nitrogen. The frozen sample in a quartz tube can be introduced in a nitrogen dewar (full with liquid nitrogen) and the whole system introduced in the cavity for scanning the EPR spectrum (EPR detects only paramagnetic material and thus, it can be performed with turbid solutions and with solids) (Fig. 4A). The time spent between taking the sample and freezing it may favor the detection of long-lived species, such as iron nitrosyl complexes [58]. Manipulation of tissue samples should be avoided because cutting, grinding, homogenization and lyophilization are all known to introduce artifacts that may be difficult to control [59]. Interestingly, it was recently shown that mechanical stress on collagen produces radicals and, subsequently, H_2O_2 [60].

The major drawback of frozen samples is the interpretation and assignment of the resulting EPR spectra. Indeed, when a radical is immobilized in a frozen matrix a multitude of superimposed spectra (one for each orientation of the radical in the magnetic field) lead to

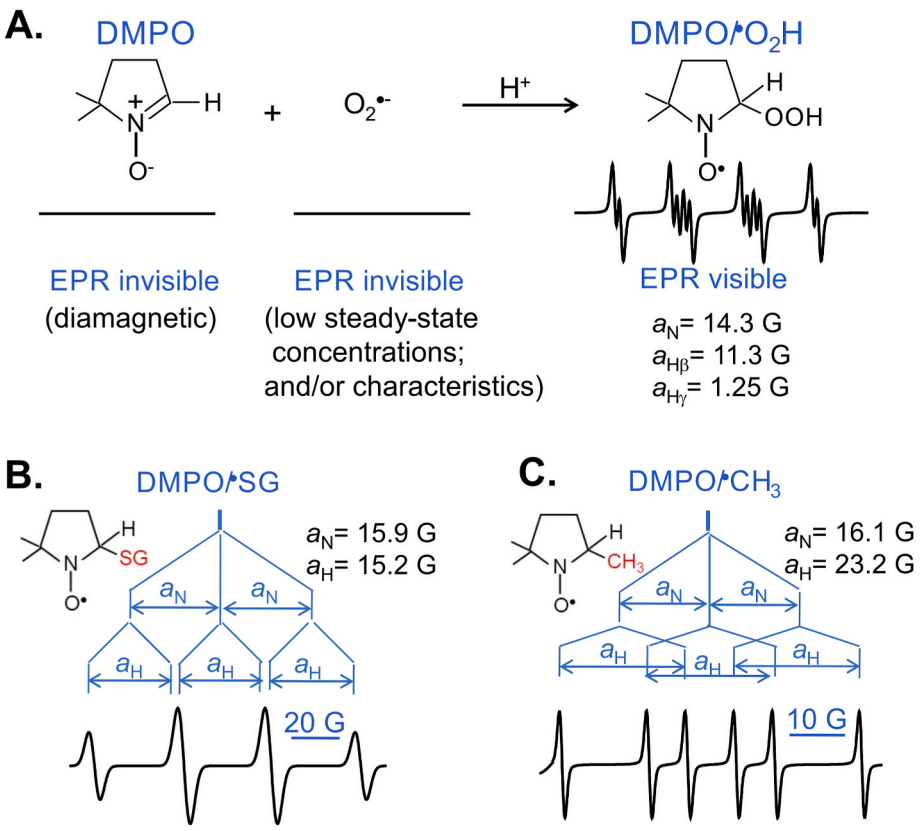

Fig. 7. A. Schematic illustration of the basis of the spin trapping method. **B.** EPR spectrum of the DMPO/$^{\bullet}$SG radical adduct accompanied by its structure, fork scheme and hyperfine splitting constants. **C.** The same as **B.** for the DMPO/$^{\bullet}CH_3$ radical adduct. The spectra are simulations created with the software WinEPR SimFonia (Bruker) using the specified hyperfine constants.

broad and composite line(s) centered at *g* around 2.0. Indeed, one of the unique characteristics of EPR spectra is that in many cases the *g* values (g_{xx}, g_{yy}, g_{zz}) and hyperfine constant values (a_{xx}, a_{yy}, a_{zz}) depend on the direction of the magnetic field relative to the molecular axes (Fig. 6, inset). This spectral anisotropy was not discussed before because we were addressing relatively small free radicals in aqueous solutions. The rapid and random rotation of these small radicals in a non-viscous solvent, such as water, averages all the hyperfine constant and *g* values, yielding EPR spectra with narrow linewidths in which the hyperfine constants are well-resolved and the spectra can be interpreted in a relatively simple manner as discussed above. In fact, the EPR spectrum of di-*t*-butyl nitroxide in a non-viscous solvent (Fig. 6A bottom spectrum) shows the characteristic isotropic three-line spectrum of a nitroxide radical (compare with Fig. 2D), from which the isotropic a_N value is easily obtained. However, di-*t*-butyl nitroxide randomly and rigidly oriented in a frozen solution yields a spectrum with much broader and distorted lines, reflecting spectra from all different directions (with the corresponding (g_{xx}. g_{yy}, g_{zz} and a_{xx}, a_{yy}, a_{zz}) values superimposed (Fig. 6A, top spectrum) [15,61]. In the latter case, only the largest hyperfine splitting can be measured (a_{zz}) because the main molecular axis of a nitroxide radical is in the z direction, since the unpaired electron is principally localized in the $p\pi$ orbital on the N atom (Fig. 6A, inset). The anisotropy of EPR spectra is the basis of the spin labeling method. It is also crucial to interpret the EPR spectra of transition metal ions (see *4.*) and to recognize spin trapping of biomolecule-derived (or high molecular weight) radicals (Fig. 6B) (see *3.4.*).

In the case of low temperature EPR, the spectral anisotropy is not necessarily a problem in systems with only a single or few components (for instance, studies on isolated enzymes), but it can be a major problem in a complex biological system, except in the case of metal ions and metal ion complexes.

3.4. EPR spin trapping

Initially developed to facilitate the detection of radicals in chemical systems [62,63], EPR spin trapping became the most successful methodology to detect radicals in biological systems including cells, organelles and experimental animals [64,65]. In a EPR spin trapping experiment, a transient radical reacts with a spin trap (usually a nitrone or a nitroso compound) to produce a more stable radical adduct (a nitroxide) that accumulates and reaches concentrations detectable by EPR (Fig. 7A). The method is indirect since the detected radical is not the primary radical, but a radical adduct, bringing in some limitations that should be taken into consideration. Nevertheless, the EPR spin trapping methodology has numerous advantages when judiciously applied. It requires small samples and permits detection of radicals of great biological interest with characteristics (short lifetime and broad linewidths) that preclude their detection in aqueous solution at room temperature by other EPR methodologies. Examples include $O_2^{\bullet -}$ (Fig. 7A), HO$^{\bullet}$ (Fig. 2A), ROO$^{\bullet}$ (peroxyl) [55] and RS$^{\bullet}$ radicals (*e.g.* glutathionyl (GS$^{\bullet}$) and cysteinyl (CysS$^{\bullet}$) (Fig. 7B) [52,66]. The technique also permits detection of high molecular weight radicals, such as those produced from the one-electron oxidation of biomolecules (proteins, DNA, lipids and polysaccharides) [67,68].

As mentioned above, two-types of spin traps have been mostly used, nitrone and nitroso spin traps (Fig. 8A). Among the first, we included in the figure the nitrones, DMPO (5,5-dimethyl-1-pyrroline N-oxide) and DEPMPO (5-diethoxyphosphoryl-5-methyl-1-pyrroline N-oxide) and the acyclic nitrone, POBN (POBN (α-(4-pyridyl-1-oxide)-N-tert-butylnitrone) and PBN (N-tert-butyl-α-phenylnitrone), which is similar but more hydrophobic than POBN. Among the nitroso spin traps, those that have been most used are MNP (2-methyl-2-nitrosopropane) and DBNBS (3,5-dibromo-4-nitrosobenzene sulfonic acid).

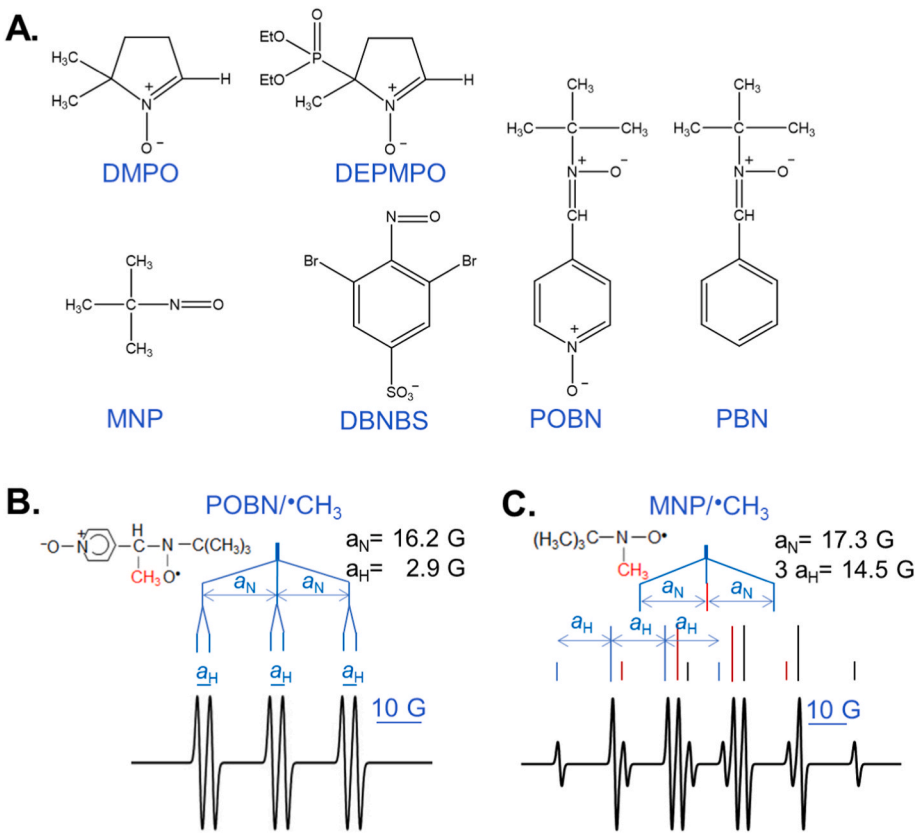

Fig. 8. A. Structure of the commonly used spin traps as specified. **B.** EPR spectrum of the POBN/$^{\bullet}CH_3$ radical adduct accompanied by its structure, fork scheme and hyperfine splitting constants. **C.** The same as **B.** for the MNP/$^{\bullet}CH_3$ radical adduct. In the latter case, the fork scheme was incomplete and with a different color for the splitting of each H nucleus for clarity. The spectra are simulations created with the software WinEPR SimFonia (Bruker) using the specified hyperfine constants.

Nitrone spin traps form long-lived adducts with a wide range of radicals (C-, O-, S- and N-centered radicals) and have low toxicity [69,70], justifying their extensive use in experimental animals [64,71,72]. However, since the radical adds to the C atom adjacent to the incipient nitroxide group, eventual magnetic nuclei present in the radical will be too distant from the nitrogen-oxygen orbital containing the unpaired electron (Fig. 6, inset) to influence the radical adduct spectrum (Fig. 7A; 7B; 8B). Consequently, most radical adducts have similar spectra, six lines of the same intensity (1 N and 1H) and small variations in *g*, a_N and a_H values, with some exceptions. For instance, the cyclic nitrones DMPO and DEPMPO reacting with O- and S-centered radicals render radical adducts showing considerable variations in the a_H values (compare Figs. 2A, 7A and 7B). However, these variations do not hold for distinct C-centered radicals, such as DMPO/$^{\bullet}CH_3$ (Fig. 7C) and, for instance, DMPO/$^{\bullet}CHOHCH_3$ (a_N = 16.1 G; a_H = 23.0 G) [73]. DEPMPO radical adducts have an additional coupling due to the presence of an additional magnetic nucleus, P (I = ½) (Table 2), which has a large hyperfine splitting constant (around 50 G) [74]. The acyclic nitrones PBN and POBN give quite stable radical adducts, but all of them have similar 6-line spectra with subtle variations in both a_N and a_H values (see, for instance, Fig. 8B).

In contrast to nitrone spin traps, nitroso spin traps give long-lived radical adducts almost exclusively with C-centered radicals and MNP is light sensitive and prone to artifacts [55,63]. Nevertheless, since the radical adds directly to the N of the incipient nitroxide group, eventual magnetic nuclei present in the radical are close enough to interact with the free electron, resulting in additional hyperfine couplings in the EPR spectrum of the radical adduct and, consequently, in more structural information about the trapped radical. This is exemplified in Fig. 8C that shows the structure, the partial fork scheme (for clarity) and the EPR spectrum of the MNP/$^{\bullet}CH_3$ radical adduct, resulting from the addition of $^{\bullet}CH_3$ to MNP. The spectrum is a triplet (1:1:1) of quartets (1:3:3:1) resulting from 1 N to 3 equivalents H, respectively. Therefore, for trapping C-centered radicals *in vitro*, nitroso spin traps might be a good choice because they provide more information about the identity of the trapped radical and usually react more rapidly than nitrone spin traps [16]. However, in experiments with cell cultures and animals, nitroso spin traps should not be used because they are highly toxic [70].

Up to this point we summarized the fundamentals of spin trapping, exemplifying radical adduct formation, spectra and EPR parameters (a_N and a_H values) for different radical adducts in aqueous solutions (Figs. 7 and 8). However, it should be emphasized that the a_N and a_H values of each radical variy depending on the solvent (environment) in which it is in. A compilation of the parameters (a_N and a_H values) of radical adducts for each available spin trap with radical intermediates reported in the literature in various solvents is found at the NIEHS website: https://tools.niehs.nih.gov/stdb/index.cfm. Such compilation may help in the interpretation of EPR spectra obtained in spin trapping experiments.

The choice of an adequate spin trap is crucial for the success of spin trapping experiments as resumed above. If there are previous hints that the radical of interest is an O-centered radical, there is no use in trying nitroso spin traps to detect it. Cyclic nitrones, DMPO or DEPMPO would be better choices.

The case of $O_2^{\bullet-}$ is a special one. Not particularly reactive towards organic molecules, $O_2^{\bullet-}$ also reacts with all spin-traps with quite small second order rate constants (in the range of 1 to <100 M^{-1} s^{-1}), producing short-lived superoxide radical adducts [16]. The advantage of DEPMPO over DMPO is the higher persistence of the DEPMPO/$^{\bullet}OOH$ (approximately 15 times at pH 7.0) as compared to that of DMPO/$^{\bullet}OOH$ [74]. In addition to DEPMPO, there are other cyclic nitrone spin traps that are able to give radical adducts of $O_2^{\bullet-}$ that are more persistent than DMPO/$^{\bullet}OOH$ in chemical and enzymatic systems [16,75]. In cells, the

persistence of $O_2^{\bullet-}$ radical adducts likely depends on cell type and the inducer of $O_2^{\bullet-}$ production [75].

It should be added that $O_2^{\bullet-}$ superoxide radical adducts are hydroperoxides (see, for instance DMPO/$^{\bullet}$OOH, Fig. 7A), which can be reduced by chemical and cellular reductants, producing the corresponding hydroxyl radical adduct (DMPO/$^{\bullet}$OH (Fig. 3A) in the case of DMPO/$^{\bullet}$OOH). Consequently, spin trapping experiments with DMPO anticipated to show $O_2^{\bullet-}$ formation, may display only the DMPO/$^{\bullet}$OH spectrum (and the same is valid for DEPMPO and the other spin traps developed to trap $O_2^{\bullet-}$) [75]. In these cases, control experiments in the presence of superoxide dismutase and catalase may help distinguishing the source of the $^{\bullet}$OH radical adduct. The most extensively used spin trap is DMPO and the DMPO/$^{\bullet}$OH can be produced not only from trapping of the HO$^{\bullet}$ and decay of DMPO/$^{\bullet}$OOH, but also from trapping of the $CO_3^{\bullet-}$ (carbonate radical) [76,77]. Which radical is trapped can be determined by control experiments in the presence of dimethyl sulfoxide (DMSO) that does not react with $CO_3^{\bullet-}$, but reacts with $^{\bullet}$OH to produce DMPO/$^{\bullet}CH_3$ (Fig. 7C), the EPR spectrum of which is distinctive from that of DMPO/$^{\bullet}$OH (Fig. 3A).

Another special case is the signaling radical NO$^{\bullet}$. Unreactive towards organic molecules [12], NO$^{\bullet}$ also does not react with nitrone and nitroso spin traps [78]. In contrast, nitronyl nitroxides, such as carboxy-PTIO (2-(4-carboxyphenyl)-4,4,5,5-tetramethylimidazoline-1-oxyl-3-oxide), have been used as NO$^{\bullet}$ trapping agents [79]. These radicals react with NO$^{\bullet}$ to produce other radicals (iminonitroxides), which have EPR spectra markedly different from that of the parent nitronyl nitroxide, permitting the distinction between the two radicals and detection of NO$^{\bullet}$ formation [78]. Currently, nitronyl nitroxides are more often used as NO$^{\bullet}$ scavengers than detectors. And NO$^{\bullet}$ is either detected by methodologies unrelated to EPR [80] or is detected by direct EPR as nitrosyl complexes from endogenous or exogenous iron centers (see *4.1.*).

Spin trapping of radicals produced from the one-electron oxidation of proteins, nucleic acids and other high molecular weight biomolecules render radical adducts, the EPR spectra of which are broad and characteristic of slowly tumbling (partially immobilized) nitroxides (Fig. 6). However, there are exceptions due to a number of factors, which have been better studied in the case of proteins. It has been shown that the mobility of protein radical adducts as assessed by the overall width of the spectral features (the $2A_{zz}$ value in Fig. 6) does not correlate with the molecular mass of the protein [67,68]. For instance, spin trapping experiments with DBNBS of the oxidation of two proteins, lysozyme (Lysoz) (14.03 kDa) or ribonuclease (Rnase) (13.68 kDa), by myeloperoxidase/H_2O_2/NO_2^- produced DBNBS/$^{\bullet}$Tyr-protein adducts of different mobility despite both proteins possessing similar sizes [81]. Indeed, the $2A_{zz}$ of DBNBS/$^{\bullet}$Tyr-Lysoz (Fig. 6B top spectrum) was much higher than that of DBNBS/$^{\bullet}$Tyr-Rnase (Fig. 6B bottom spectrum) (62.5 G and 27.4 G, respectively) [81]. This fact is consistent with the local environment of the nitroxide moiety determining the overall mobility of the adduct, rather than the tumbling rate of the protein as a whole [67,68]. Nitroso spin traps were the most employed to investigate protein radicals, particularly DBNBS because of its stability and higher water solubility. DMPO has also been used, particularly to detect protein-thiyl radicals [82,83].

Spin trapping alone cannot identify the protein residue in which the radical is localized, but protein-radical adducts can be submitted to enzymatic proteolysis and subsequently analyzed by HPLC-mass spectrometry to reveal the trapped protein residue(s) (see, for instance, Ref. [84]). In the case of the experiments shown in Fig. 6B, an unspecific tyrosyl residue of both proteins was inferred as the trapped radical from the properties of the proteins and of their corresponding DBNBS radical adducts [81].

It should be stressed that EPR spin trapping considerably expands its horizons when associated with mass spectrometry (see, for instance, Refs. [77,84,85]), isotopic labeling (see, for instance, Refs. [71,86]) and immunological techniques alone [87,88] or associated with molecular magnetic resonance imaging (mMRI) [89,90].

3.4.1. *Spin trapping: experimental hints*

As our goal is to encourage those new to the redox field to consider EPR methodologies, we have included some experimental tips that are available in the literature but are not always easy to find.

To favor the spin trap over endogenous targets for the primary radical, usually high concentrations of spin traps (tents of mM and hundreds of mM for nitroso and nitrone traps, respectively) are employed in spin trapping experiments. Therefore, high purity spin traps are crucial to avoid artifacts due to impurities, particularly paramagnetic ones. Most commercial spin traps have high purity but sometimes it may not be enough. DMPO can be purified by low pressure distillation or through filtration of a concentrated DMPO aqueous solution ($10H_2O$:1 DMPO v/v) through activated charcoal [91]. After determination of the purified solution concentration ($\varepsilon_{234} = 7.70 \times 10^3$ M^{-1} cm^{-1} in ethanol), it can be aliquoted under N_2 and stored at 77 K till use. MNP is commercially obtained as a solid dimer that dissociates to the blue monomer in solution [63]. We usually make a stock solution of MNP in acetonitrile that should be maintained protected from light, before diluting it in the aqueous samples (also protected from light). After trying several commercial batches of DBNBS without success, we

Table 3
Metalloproteins and g values.

Metalloprotein	Metal ion	g values	Ref
Guanylate cyclase[a]	Fe(III)	g = 6.36, 5.16, and 2.0	[99]
Nitrosyl guanylate cyclase[a]	Fe(II)	g = 2.76, 2.029, and 2.005	[100]
Methaemoglobin	Fe(III)	high spin - g = 6 low spin - g = 2.855, 2.226, and 1.794	[101]
Fe Superoxide Dismutase[b]	Fe(III)	g = 4.7, 4.0, and 3.7	[102]
Cu–Zn Superoxide Dismutase[a]	Cu(II)	g = 2.265, 2.108, and 2.023	[103]
Photosystem II	Mn(II-IV) clusters	g = from 2 to 4 depending on S state	[104]
Xanthine Oxidase[c]	Mo(V)	g = 1.986, 1.968, and 1.966	[105]
[FeFe] hydrogenase (oxidized)[d]	Fe(I-II) cluster	g = 2.056, 2.008, and 2.008	[106]
Ferric uptake regulatory protein (reduced)[b]	Fe(II-III) sulfur cluster	g = 1.91, 1.94, and 2.00	[107]
Hydroxylamine Oxidase (DnfA)[e]	Fe(II-III) sulfur cluster	g = 1.912, 1.876, and 1.793	[108]

[a] from bovine.
[b] from *Escherichia coli*.
[c] from unpasteurized cow's milk.
[d] from *Chlamydomonas reinhardtii*.
[e] *Alcaligenes ammonioxydans*.

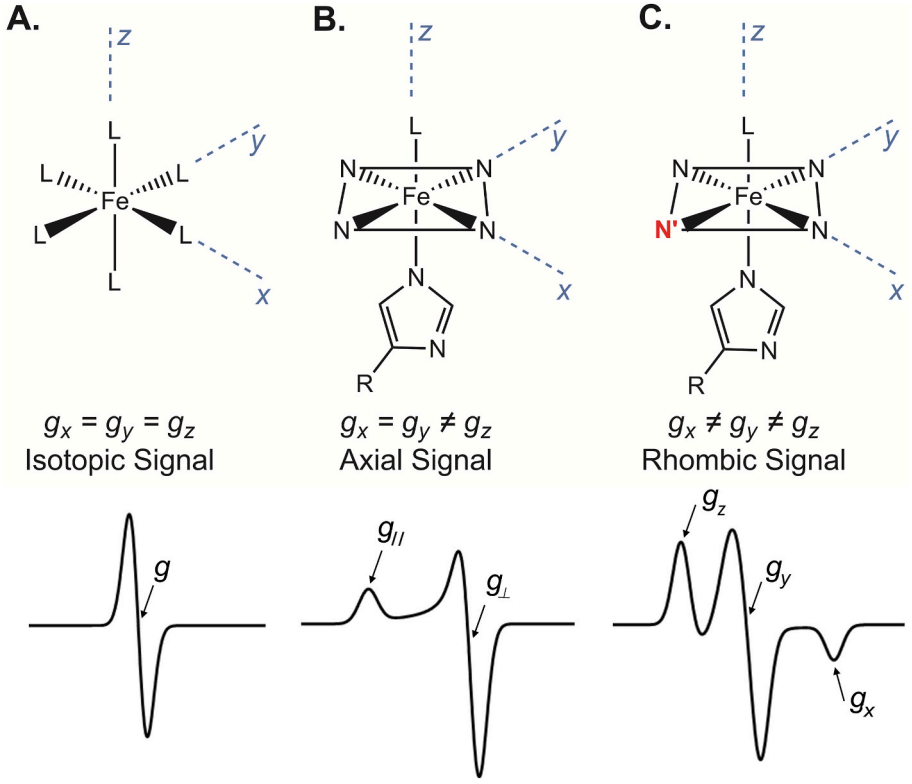

Fig. 9. Paramagnetic anisotropy illustrated with a simplified representation of metal complexes of **A)** Isotropic, **B)** Axial, and **C)** Rhombic symmetry. The N′ represent an inequivalent nitrogen atom. The spectra are simulations created with the software WinEPR SimFonia (Bruker).

usually synthesize it for our use, employing a simple method previously described [92].

In the case of spin trapping experiments with cells, organelles and experimental animals, the possibility of reduction and oxidation of the radical adduct should be considered. Indeed, radical adducts (nitroxides, N–O$^{\bullet}$) can be reduced by cellular reductants to hydroxylamine (N–OH) or oxidized by cellular oxidants to oxoammonium cation (N^{+}=O), both of which are no longer detectable by EPR (diamagnetic; EPR silent). Reduction of radical adducts is apparently more frequent in cells and biological fluids than oxidation [93]. Therefore, it may be a good strategy to maintain cells in permeable tubes to maintain aeration or to use a controlled atmosphere [75]. Likewise, in the case of *in vivo* spin trapping experiments it may be relevant to treat samples of bile and blood drawn from experimental animals with ascorbate oxidase (to oxidize endogenous ascorbate). Alternatively, these samples may be treated with O_2 or with ferricyanide to re-oxidize eventually formed hydroxylamines to the corresponding radical adducts [72,86].

3.5. Spin scavenging

More recently a method that has been called spin scavenging was developed based on the rapid oxidation of hydroxylamines (which are diamagnetic and therefore, EPR silent) by radicals to produce nitroxide radicals [94]. Highly substituted 5- or 6-membered ring species are most commonly used as they render persistent nitroxide radicals. These hydroxylamines typically react with $O_2^{\bullet-}$ with much higher rate constants than DMPO and DEPMPO and therefore, may be useful to detect $O_2^{\bullet-}$ formation [95,96], particularly because superoxide dismutase addition may prove $O_2^{\bullet-}$ formation. However, hydroxylamine oxidation to nitroxides is mediated by a variety of radicals and other biological oxidants, such as transition metal ions and peroxidase enzymes [16]. This complete lack of specificity considerably limits the applicability of spin scavenging.

4. EPR of metal ion complexes and metalloproteins

Numerous metal complexes present in biological systems have been identified, quantified, and structurally characterized thanks to EPR spectroscopy. Different than radicals, transition metals can have more than one unpaired electron ($S = n/2$, where n is the number of unpaired electrons) generally located in d-orbitals. This localization results in a strong interaction between the magnetic momentum and the orbital angular momentum of d-electron(s). Also, the angular nature of d-orbitals can specifically interact with the metal ion ligands giving rise to anisotropic EPR spectra that reflect the 3D electronic structure of the complex [97,98]. Therefore, the g values (g_x, g_y, g_z) for metal centers are considerably different from that of the free electron and are markedly defined by the direction of the magnetic field relative to the molecular axes of the complexes, their geometry and nature of the metal ligands (Table 3).

To exemplify, we may consider a single crystal of a metal complex ($S = 1/2$) presenting an octahedral structure with six identical ligands (Fig. 9A) positioned at different orientations of an external magnetic field. It will give rise to an isotropic EPR signal ($g_x = g_y = g_z$). However, the signal shape changes in cases where the octahedral structure is maintained, but the ligands are different such as in ferric heme structures, like ferric hemoglobin, ferric guanylyl cyclase, or ferric cytochrome *c*. In these complexes, the low-spin ferric heme ($S = 1/2$) exhibits a porphyrin in *xy* plane (simplified in Fig. 9B by four N at equal distance from Fe) and N (His) and L (variable ligand) as axial ligands (z-axis). When axis *x* or *y* of this complex is placed parallel to an external magnetic field, the values of g_x and g_y are equal because the simplified porphyrin plane structure is symmetric. Meanwhile, when the z-axis is placed along the external magnetic field, the g_z will have a different value determined by N and L ligands resulting in an axial spectrum ($g_x = g_y \neq gz$ or $g\perp$ and $g_{//}$). If the porphyrin N are not equivalent (Fig. 9C), either because of the presence of different substituents in the porphyrin ring or because of specific surrounding chemical interactions, then the

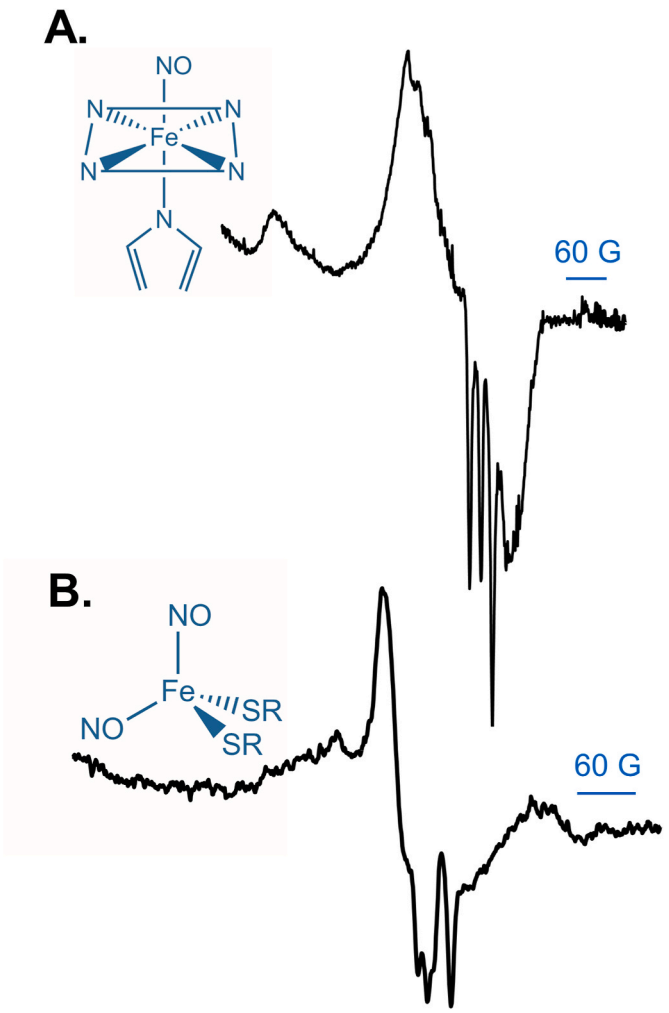

Fig. 10. Representative low-temperature EPR spectra of: **A)** Hemoglobin-nitrosyl complexes obtained in blood taken by cardiac punction from rats 6 h after LPS (0.8 mg/kg) administration [105]. **B)** Iron dithiol dinitrosyl complexes obtained from footpads of resistant mice infected with *L. amazonensis* [58]. Both spectra were modified from the cited references with permission.

EPR signal becomes rhombic ($g_x \neq g_y \neq g_z$). Most of the metal complexes of interest to biology are not analyzed as a single crystal, but rather as a powder, a frozen solution or even in room temperature solution. Frozen solutions at very low temperature ($\leq$77 K) are usually preferred due to spin-orbital coupling and other factors contributing to the short relaxation time (to decay from the high to the low energy state) of electron spins.

In addition to the electronic configuration (number of unpaired electrons), the geometry of the complex and the nature of the ligands, the EPR signal for transition-metal ions can also exhibit hyperfine interaction between the unpaired d-electron(s) and surrounding nuclei with magnetic moment (Table 1), characteristics that very often make the interpretation of EPR spectra for metal ions more complex than for radicals.

4.1. EPR of NO•-iron complexes

These EPR spectra are a good model to exemplify how the singular EPR signal shape of metal ion complexes can become a valuable strategy to detect, quantify, and characterize metalloproteins in biological media. Since NO• is highly reactive towards metal centers, it is detectable by direct EPR of frozen tissues and cells as nitrosyl complexes of endogenous heme and non-heme iron (arising from the iron-sulfur

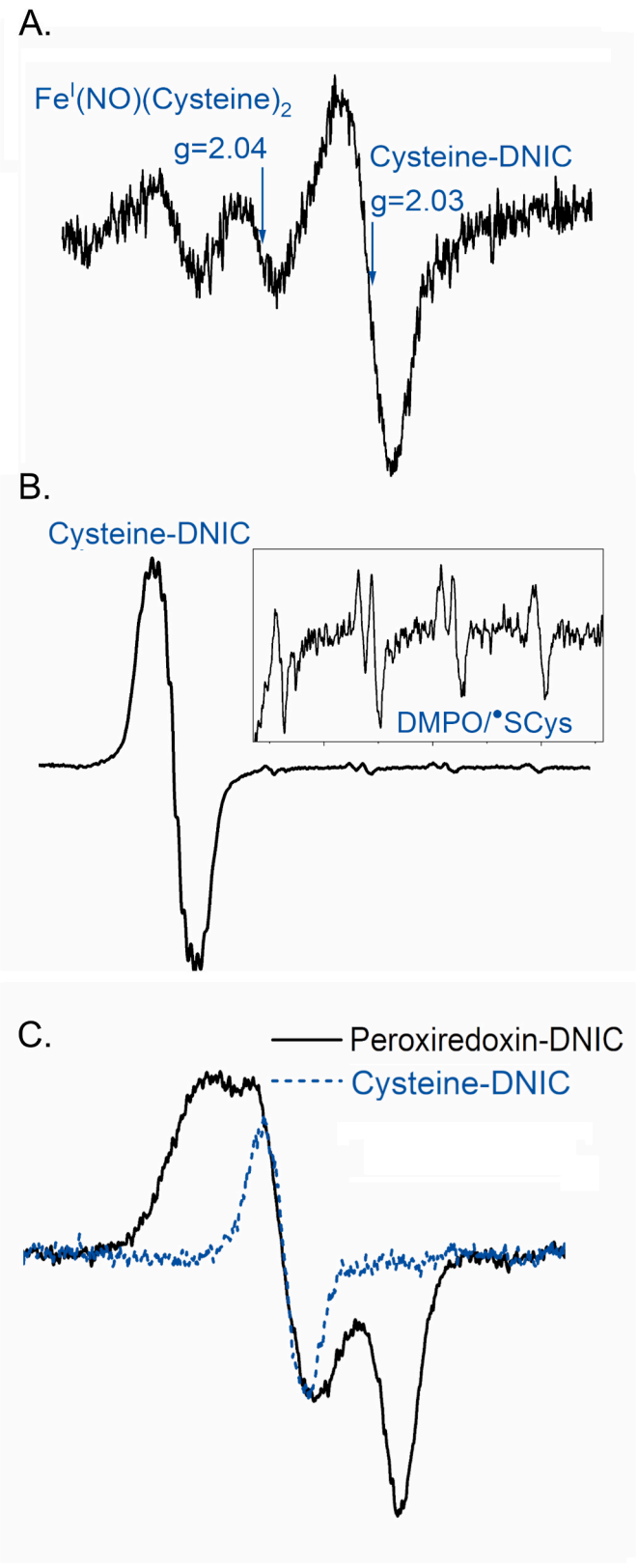

Fig. 11. Representative room temperature EPR spectra **A)** acquired during the cysteine-DNIC assembly 0.1 s after mixing a solution of NO• with a solution of Fe(II) and Cys in a continuous flow cavity (see Fig. 4C). **B)** acquired using a flat cell immediately after the mixing of Fe(II), NO•, Cys and the spin trap DMPO. The inset shows the expanded region of the EPR signal of the DMPO/•Cys radical adduct. **C)** acquired using a flat cell for the low-molecular-weight cysteine-DNIC and the peroxiredoxin-bound DNIC as specified. The spectra shown in A) and B) were modified from Ref. [66] with permission.

clusters or the labile iron pool), particularly in rodents, which have a robust $NO^{\bullet}$ component in their infectious and inflammatory responses [58,78,109].

The reaction of ferrous heme and $NO^{\bullet}$ gives rise to nitrosyl heme complexes, such as the nitrosyl hemoglobin ($Hb(Fe^{II})NO$) detected by EPR in blood taken by cardiac punction from rats that had $NO^{\bullet}$ production trigged by LPS administration (Fig. 10A) [110]. This figure shows a rhombic spectrum, due to electronic configuration, geometry, and ligand nature (Fig. 9C), which also exhibits a defined three-line hyperfine splitting in the z-axis as a consequence of the hyperfine interaction between the unpaired d-electron and the ^{14}N ($I = 1$) from $NO^{\bullet}$ [111,112]. Another example is the characteristic axial EPR signal at $g = 2.03$ (Fig. 10B) ubiquitously found in cells and tissues under conditions of inducible $NO^{\bullet}$ synthase (iNOS) activation [58,113,114]. Such signal results from the reaction between $NO^{\bullet}$ and non-heme irons, such as the labile iron pool and iron-sulfur clusters, which have as final products dinitrosyl iron complexes (DNICs, $Fe^{I}(NO)_2(RS)_2$). The DNICs are abundant $NO^{\bullet}$ metabolites described as $\{Fe^{I}(NO^{\bullet})_2\}^9$, in which the spins of the two $NO^{\bullet}$ ($S = 1/2$) and the Fe^{I} ($S = 3/2$) are antiferromagnetic coupled to give $S_t = 1/2$. Antiferromagnetic coupling occurs when the metal center electrons have spins in opposite direction to other system spins, generating a smaller total spin [115,116].

EPR spectroscopy associated with the methodological approaches described before was fundamental to elucidate the mechanisms of DNICs formation, determine DNICs levels, and ligand composition [66, 117–121]. For instance, direct continuous-flow EPR was employed to acquire spectra 0.1 s after mixing solutions of $NO^{\bullet}$ and Fe(II) with thiols. The obtained spectra exhibited a triplet signal at $g = 2.04$, allowing to identify the Fe^{I} mononitrosyl complex ($Fe^{I}(NO)(RS)_2$) as the precursor of DNIC ($g = 2.03$) formation (Fig. 11A). Also, spin trapping and static direct EPR combined demonstrated the parallel formation of DNICs and thiyl radicals, the latter was detected by formation of the corresponding DMPO/$RS^{\bullet}$ adducts (Fig. 11 B) [66].

Direct EPR at room temperature can distinguish low molecular weight DNICs and protein-bound-DNICs based on the anisotropic properties [118,121,122]. Fig. 11C shows that room temperature EPR spectra of DNICs containing glutathione as ligand (DNIC-GS) exhibit a single symmetrical line at $g = 2.03$ because in aqueous media at room temperature the rapid tumbling of this molecule generates a fully averaged or isotropic *g* value. In contrast, DNICs containing proteins, such as albumin, glutathione transferases, or peroxiredoxin 1 as ligand exhibit anisotropic EPR, since the coordination of a high molecular weight molecule results in a slower rotation rate [118].

The high reactivity between $NO^{\bullet}$ and metal centers was used to develop $NO^{\bullet}$-traps such as water-soluble Fe(II) dithiocarbamate complexes (e.g. those derived from diethyldithiocarbamate (DETC) and N-methyl-D-glucamine (MGD)) which interact with $NO^{\bullet}$ to produce EPR-detectable complexes at room temperature and have been extensively used *in vitro* and *in vivo* to quantify NO• (reviewed in Refs. [78,123]). Associated with isotopic substitution (^{14}N by ^{15}N), this methodology permits to distinguish whether $NO^{\bullet}$ is being produced primarily from arginine oxidation (via nitric oxide synthases) or NO_2^- or NO_3^- reduction [124].

5. Other applications of EPR related to the redox field

Many EPR applications that are of interest to investigators in the redox field were not presented to maintain the focus on the main objectives of this review, but some of them deserve mention. For instance, EPR oximetry due to the great influence of O_2 concentrations on redox reactions and the fact that homeostasis of aerobic organisms depends on optimal cellular and tissue O_2 levels. As the name suggests, EPR oximetry refers to the measurement of O_2 concentration by EPR [125]. Although O_2 occurs naturally as a triplet radical (has two unpaired electrons in the ground state), it is not directly detectable by EPR when dissolved in liquids due to its extremely short relaxation time. Therefore, measurements of O_2 concentration by EPR require the use of a stable radical (spin probe). O_2 interacts with the spin probe (spin-spin interaction), resulting in the broadening of the linewidths of the EPR signal of the probe in a manner that makes the linewidths linearly correlate with O_2 content (concentration or pressure) [126]. An easy way to observe the effect of O_2 concentration on the linewidths of the EPR spectrum of a spin probe is to compare the linewidths of a stable nitroxide in aqueous solutions and in benzene, which contains roughly 10 times more dissolved O_2 than water at standard atmosphere. Historically, EPR oximetry started with the observation of the effect of oxygen concentrations on the EPR spectra of a spin label in 1976 [125]. Since then, EPR oximetry has continuously evolved with the development of novel spin probes, methods and instrumentation, mainly due to the many clinical potentialities of the technique [125,126].

We mentioned before that hindered nitroxides have long been employed as spin probes (spin labels) in biophysical studies constituting the basis of the spin labeling technique (see *3.1.)*. Initially, covalent modification of lipids at specific sites with spin labels to study the properties of membranes was more widespread [38–40], but soon similar modifications in proteins became common [127,128]. Not surprisingly, the spin labeling technique has also been used to approach questions of interest to redox investigators. For instance, the interaction among O_2 and spin probes stimulated the incorporation of spin labeled lipids in membranes to study O_2 diffusion through membrane models [129] and biological membranes [130,131]. The localization of vitamin E in membranes and the mechanism by which it protects against lipid peroxidation was examined by incorporating spin labeled lipids in liposomes [132]. Other examples are available in the literature, such as the incorporation of a spin labeled lipid in membranes of: (i) rat brain synaptosomes and mitochondria to follow the effect of caloric restriction on membrane fluidity and oxidation [133]; (ii) erythrocytes of hypertense patients to study $NO^{\bullet}$ effects on membrane fluidity [134].

6. Conclusion

There are many excellent reviews about the detection of free radical metabolites by EPR in the literature and some of them are included in the references. The difference here is that we attempted to explain in a didactic manner not only the EPR phenomenon, but also the interpretation of the EPR spectra of radicals, metalloproteins and transition metal ion complexes. We certainly oversimplified several aspects, but provided references to fill the gaps we left. Our goal was to introduce EPR methodologies to the beginners in the redox field, in particular to those in the field of redox biology that is overlooking EPR as pointed out in the introduction. However, EPR methodologies contributed to development of the redox area since its early days and will certainly contribute to its future advances. Afterall, the uniqueness of EPR spectroscopy in identifying and quantifying (within reasonable limits) free radicals, metalloproteins and transition metal ion complexes makes it essential for studying redox mechanisms underlying chemical as well biological phenomena.

Funding

The authors acknowledge financial support from Sao Paulo Research Foundation (FAPESP, Grants 13/07937–8 and 19/17483–0) and National Council for Scientific and Technological Development (CNPq, Grant 301597/2019-7).

Author contributions

OA, DRT and EL conceived the article; EL selected the material for the figures and made the spectra simulations; DRT wrote about metalloproteins and metal ion complexes; OA wrote the final version; all authors approved the final version.

Declaration of competing interest

The authors declare that they have no known competing financial interests or personal relationships that could have appeared to influence the work reported in this paper.

Acknowledgement

The graphical abstract was constructed using the software from Biorender.com.

References

[1] R. Gerschman, D.L. Gilbert, S.W. Nye, P. Dwyer, W.O. Fenn, Oxygen poisoning and X-irradiation: a mechanism in common, Science 119 (1954) 623–626, https://doi.org/10.1126/science.119.3097.623.

[2] J.M. McCord, I. Fridovich, Superoxide dismutase. An enzymic function for erythrocuprein (hemocuprein), J. Biol. Chem. 244 (1969) 6049–6055, https://doi.org/10.1016/S0021-9258(18)63504-5.

[3] Helmut Sies, Introductory Remarks. Oxidative Stress, first ed., Academic Press, London, 1985, pp. 1–8.

[4] R. Furchgott, J. Zawadzki, The obligatory role of endothelial cells in the relaxation of arterial smooth muscle by acetylcholine, Nature 288 (1980) 373–376, https://doi.org/10.1038/288373a0.

[5] L.J. Ignarro, G.M. Buga, K.S. Wood, R.E. Byrns, G. Chaudhuri, Endothelium-derived relaxing factor produced and released from artery and vein is nitric oxide, Proc. Natl. Acad. Sci. USA 84 (1984) 9265–9269, https://doi.org/10.1073/pnas.84.24.9265.

[6] M. Suradesen, Zu-Xi Yu, Victor J. Ferrans, Kaikobad Irani, Toren Finkel, Requirement for generation of H2O2 for platelet-derived growth factor signal transduction, Science 270 (1995) 296–299, https://doi.org/10.1126/science.270.5234.296.

[7] J.R. Stone, An assessment of proposed mechanisms for sensing hydrogen peroxide in mammalian systems, Arch. Biochem. Biophys. 422 (2004) 119–124, https://doi.org/10.1016/j.abb.2003.12.029.

[8] H.J. Forman, M. Maiorino, F. Ursini, Signaling functions of reactive oxygen species, Biochemistry 49 (2010) 835–842, https://doi.org/10.1021/bi9020378.

[9] Helmut Sies, P Jones. Dean, Reactive oxygen species (ROS) as pleiotropic physiological signalling agents, Nat. Rev. Mol. Cell Biol. 21 (2020) 363–383. https://doi.org/10.1038/s41580-020-0230-3.

[10] C.C. Winterbourn, Are free radicals involved in thiol-based redox signaling? Free Radic. Biol. Med. 80 (2015) 164–170, https://doi.org/10.1016/j.freeradbiomed.2014.08.017.

[11] A. Martínez-Ruiz, S. Cadenas, S. Lamas, Nitric oxide signaling: classical, less classical, and nonclassical mechanisms, Free Radic. Biol. Med. 51 (2011) 17–29, https://doi.org/10.1016/j.freeradbiomed.2011.04.010.

[12] J.C. Toledo Jr., O. Augusto, Connecting the chemical and biological properties of nitric oxide, Chem. Res. Toxicol. 25 (2012) 975–989, https://doi.org/10.1021/tx300042g.

[13] C.C. Winterbourn, Hydrogen peroxide reactivity and specificity in thiol-based cell signalling, Biochem. Soc. Trans. 48 (2020) 745–754, https://doi.org/10.1042/BST20190049.

[14] J.A. Weil, J.R. Bolton, J.E. Wertz, Electron Paramagnetic Resonance. Elementary Theory and Practical Applications, Wiley, New York, 1994.

[15] P.F. Knowles, D. Marsh, H.W.E. Rattle, Magnetic Resonance of Biomolecules. An Introduction to the Theory and Practice of NMR and ESR to Biological Systems, 1a ed., John Wiley & Sons, 1976.

[16] C.L. Hawkins, M.J. Davies, Detection and characterisation of radicals in biological materials using EPR methodology, Biochim. Biophys. Acta 1840 (2014) 708–721, https://doi.org/10.1016/j.bbagen.2013.03.034.

[17] M.G. Bonini, R. Radi, G. Ferrer-Sueta, A.M. Ferreira, O. Augusto, Direct EPR detection of the carbonate radical anion produced from peroxynitrite and carbon dioxide, J. Biol. Chem. 274 (1999) 10802–10806, https://doi.org/10.1074/jbc.274.16.10802.

[18] O. Augusto, S. Goldstein, J.K. Hurst, J. Lind, S.V. Lymar, G. Merenyi, et al., Carbon dioxide-catalyzed peroxynitrite reactivity – the resilience of the radical mechanism after two decades of research, Free Radic. Biol. Med. 135 (2019) 210–215, https://doi.org/10.1016/j.freeradbiomed.2019.02.026.

[19] S.L. de Menezes, O. Augusto, EPR detection of glutathionyl and protein-tyrosyl radicals during the interaction of peroxynitrite with macrophages (J774), J. Biol. Chem. 276 (2001) 39879–39884, https://doi.org/10.1074/jbc.M104012200.

[20] J. Vasquez-Vivar, O. Augusto, Hydroxylated metabolites of the antimalarial drug primaquine. Oxidation and redox cycling, J. Biol. Chem. 267 (1992) 6848–6854, https://doi.org/10.1016/S0021-9258(19)50504-X.

[21] A. Motten, J. Schreiber, Correlation analysis of ESR spectra on a small computer, J. Magn. Reson. 67 (1969 1986) 42–54, https://doi.org/10.1016/0022-2364(86)90407-5.

[22] D.P. Barr, M.R. Gunther, L.J. Deterding, K.B. Tomer, R.P. Mason, ESR Spin-trapping of a protein-derived tyrosyl radical from the reaction of cytochrome c with hydrogen peroxide, J. Biol. Chem. 271 (1996) 15498–15503, https://doi.org/10.1074/jbc.271.26.15498.

[23] W.A. Pryor, Oxy-radicals and related species: their formation, lifetimes, and reactions, Annu. Rev. Physiol. 48 (1986) 657–667, https://doi.org/10.1146/annurev.ph.48.030186.003301.

[24] H. Sies, Strategies of antioxidant defense, Eur. J. Biochem. 215 (1993) 213–219, https://doi.org/10.1111/j.1432-1033.1993.tb18025.x.

[25] D.B. Medinas, G. Cerchiaro, D.F. Trindade, O. Augusto, The carbonate radical and related oxidants derived from bicarbonate buffer, IUBMB Life 59 (2007) 255–262, https://doi.org/10.1080/15216540701230511.

[26] C.C. Felix, R.C. Sealy, Electron spin resonance characterization of radicals from 3,4-dihydroxyphenylalanine: semiquinone anions and their metal chelates, J. Am. Chem. Soc. 103 (1981) 2831–2836, https://doi.org/10.1021/ja00400a056.

[27] B. Kalyanaraman, R.C. Sealy, Electron spin resonance-spin stabilization in enzymatic systems: detection of semiquinones produced during peroxidatic oxidation of catechols and catecholamines, Biochem. Biophys. Res. Commun. 106 (1982) 1119–1125, https://doi.org/10.1016/0006-291X(82)91228-1.

[28] R.P. Mason, J.L. Holtzman, Mechanism of microsomal and mitochondrial nitroreductase. Electron spin resonance evidence for nitroaromatic free radical intermediates, Biochemistry 14 (1975) 1626–1632, https://doi.org/10.1021/bi00679a013.

[29] M.J. Davies, A. Puppo, Direct detection of a globin-derived radical in leghaemoglobin treated with peroxides, Biochem. J. 281 (1992) 197–201, https://doi.org/10.1042/bj2810197.

[30] W. Bors, W. Heller, C. Michel, K. Stettmaier, Electron Paramagnetic Resonance studies of flavonoid compounds, in: G. Poli, E. Albano, M.U. Dianzani (Eds.), Free Radic. Basic Sci. Med., Birkhäuser Basel, Basel, 1993, pp. 374–387, https://doi.org/10.1007/978-3-0348-9116-5_32.

[31] W. Bors, C. Michel, K. Stettmaier, Electron Paramagnetic Resonance studies of radical species of proanthocyanidins and gallate esters, Arch. Biochem. Biophys. 374 (2000) 347–355, https://doi.org/10.1006/abbi.1999.1606.

[32] R.P. Mason, Chapter 6 - free-radical intermediates in the metabolism of toxic chemicals, Free Radic. Biol. V (1982). New York: Academic Press.

[33] P.D. Josephy, T.E. Eling, R.P. Mason, An electron spin resonance study of the activation of benzidine by peroxidases, Mol. Pharmacol. 23 (1983) 766, https://doi.org/10.1289/ehp.8564171.

[34] M. Demasi, O. Augusto, E.J.H. Bechara, R.N. Bicev, F.M. Cerqueira, F.M. da Cunha, et al., Oxidative modification of proteins: from damage to catalysis, signaling, and beyond, Antioxidants Redox Signal. 35 (2021) 1016–1080, https://doi.org/10.1089/ars.2020.8176.

[35] M. Minetti, G. Scorza, D. Pietraforte, Peroxynitrite induces long-lived tyrosyl radical(s) in oxyhemoglobin of red blood cells through a reaction involving CO2 and a ferryl species, Biochemistry 38 (1999) 2078–2087, https://doi.org/10.1021/bi982311g.

[36] M.G. Bonini, D.C. Fernandes, O. Augusto, Albumin oxidation to diverse radicals by the peroxidase activity of Cu,Zn-superoxide dismutase in the presence of bicarbonate or nitrite: diffusible radicals produce cysteinyl and solvent-exposed and -unexposed tyrosyl radicals, Biochemistry 43 (2004) 344–351, https://doi.org/10.1021/bi035606p.

[37] D.A. Svistunenko, C.E. Cooper, A new method of identifying the site of tyrosyl radicals in proteins, Biophys. J. 87 (2004) 582–595, https://doi.org/10.1529/biophysj.104.041046.

[38] H.M. McConnell, B.G. McFarland, Physics and chemistry of spin labels, Q. Rev. Biophys. 3 (1970) 91–136, https://doi.org/10.1017/S003358350000442X.

[39] S. Schreier, C.F. Polnaszek, I.C.P. Smith, Spin labels in membranes problems in practice, Biochim Biophys Acta BBA - Rev Biomembr 515 (1978) 395–436, https://doi.org/10.1016/0304-4157(78)90011-4.

[40] D. Marsh, Electron spin resonance: spin labels, in: E. Grell (Ed.), Membr. Spectrosc., Springer Berlin Heidelberg, Berlin, Heidelberg, 1981, pp. 51–142, https://doi.org/10.1007/978-3-642-81537-9_2.

[41] C.S. Wilcox, Effects of tempol and redox-cycling nitroxides in models of oxidative stress, Pharmacol. Ther. 126 (2010) 119–145, https://doi.org/10.1016/j.pharmthera.2010.01.003.

[42] M.D. Rees, S.E. Bottle, K.E. Fairfull-Smith, E. Malle, J.M. Whitelock, M.J. Davies, Inhibition of myeloperoxidase-mediated hypochlorous acid production by nitroxides, Biochem. J. 421 (2009) 79–86, https://doi.org/10.1042/BJ20090309.

[43] R.F. Queiroz, A.K. Jordão, A.C. Cunha, V.F. Ferreira, M.R.P.L. Brigagão, A. Malvezzi, et al., Nitroxides attenuate carrageenan-induced inflammation in rat paws by reducing neutrophil infiltration and the resulting myeloperoxidase-mediated damage, Free Radic. Biol. Med. 53 (2012) 1942–1953, https://doi.org/10.1016/j.freeradbiomed.2012.09.001.

[44] I. Yamazaki, Chapter 5 - free radicals in enzyme—substrate reactions, Free Radic. Biol. III (1977). London: Academic Press.

[45] D.C.D.C. Borg, An improved flow system for Electron Paramagnetic Resonance Spectrometry of aqueous solutions, Nature 201 (1964) 1087–1090, https://doi.org/10.1038/2011087a0.

[46] V. Fischer, L.S. Harman, P.R. West, R.P. Mason, Direct electron spin resonance detection of free radical intermediates during the peroxidase catalyzed oxidation of phenacetin metabolites, Chem. Biol. Interact. 60 (1986) 115–127, https://doi.org/10.1016/0009-2797(86)90021-9.

[47] D.N. Ramakrishna Rao, V. Fischer, R.P. Mason, Glutathione and ascorbate reduction of the acetaminophen radical formed by peroxidase. Detection of the glutathione disulfide radical anion and the ascorbyl radical, J. Biol. Chem. 265 (1990) 844–847, https://doi.org/10.1016/S0021-9258(19)40126-9.

[48] W.H. Koppenol, J.J. Moreno, W.A. Pryor, H. Ischiropoulos, J.S. Beckman, Peroxynitrite, a cloaked oxidant formed by nitric oxide and superoxide, Chem. Res. Toxicol. 5 (1992) 834–842, https://doi.org/10.1021/tx00030a017.

[49] J.S. Beckman, J. Chen, H. Ischiropoulo, J.P. Crow, Oxidative chemistry of peroxynitrite, Methods Enzymol. 233 (1994) 229–240, https://doi.org/10.1016/s0076-6879(94)33026-3.

[50] R.M. Uppu, W.A. Pryor, Synthesis of peroxynitrite in a two-phase system using isoamyl nitrite and hydrogen peroxide, Anal. Biochem. 236 (1996) 242–249, https://doi.org/10.1006/abio.1996.0162.

[51] C.X. Santos, M.G. Bonini, O. Augusto, Role of the carbonate radical anion in tyrosine nitration and hydroxylation by peroxynitrite, Arch. Biochem. Biophys. 377 (2000) 146–152, https://doi.org/10.1006/abbi.2000.1751.

[52] M.G. Bonini, O. Augusto, Carbon dioxide stimulates the production of thiyl, sulfinyl, and disulfide radical anion from thiol oxidation by peroxynitrite, J. Biol. Chem. 276 (2001) 9749–9754, https://doi.org/10.1074/jbc.M008456200.

[53] J. Laranjinha, E. Cadenas, Redox cycles of caffeic acid, alpha-tocopherol, and ascorbate: implications for protection of low-density lipoproteins against oxidation, IUBMB Life 48 (1999) 57–65, https://doi.org/10.1080/713803474.

[54] M.C.R. Symons, On the electron spin resonance detection of RS radicals in irradiated solids: radicals of type RSSR–, RS–SR2, and R2SSR2+, J Chem Soc Perkin Trans 2 (1974) 1618–1620, https://doi.org/10.1039/P29740001618.

[55] G.R. Buettner, R.P. Mason, Spin-trapping methods for detecting superoxide and hydroxyl free radicals in vitro and in vivo, Methods Enzymol. 186 (1990) 127–133, https://doi.org/10.1016/0076-6879(90)86101-Z. Academic Press.

[56] R. Bray, Sudden freezing as a technique for the study of rapid reactions, Biochem. J. 81 (1961) 189–193, https://doi.org/10.1042/bj0810189.

[57] P.F. Knowles, J.F. Gibson, F.M. Pick, R.C. Bray, Electron-spin-resonance evidence for enzymic reduction of oxygen to a free radical, the superoxide ion, Biochem. J. 111 (1969) 53–58, https://doi.org/10.1042/bj1110053.

[58] E. Linares, S. Giorgio, R.A. Mortara, C.X.C. Santos, A.T. Yamada, O. Augusto, Role of peroxynitrite in macrophage microbicidal mechanisms in vivo revealed by protein nitration and hydroxylation, Free Radic. Biol. Med. 30 (2001) 1234–1242, https://doi.org/10.1016/S0891-5849(01)00516-0.

[59] M.J. Davies, Direct detection of radical production in the ischaemic and reperfused myocardium: current status, Free Radic. Res. Commun. 7 (1989) 275–284, https://doi.org/10.3109/10715768909087952.

[60] C. Zapp, A. Obarska-Kosinska, B. Rennekamp, M. Kurth, D.M. Hudson, D. Mercadante, et al., Mechanoradicals in tensed tendon collagen as a source of oxidative stress, Nat. Commun. 11 (2020) 2315, https://doi.org/10.1038/s41467-020-15567-4.

[61] O.H. Griffith, A.S. Waggoner, Nitroxide free radicals: spin labels for probing biomolecular structure, Acc. Chem. Res. 2 (1969) 17–24, https://doi.org/10.1021/ar50013a003.

[62] E.G. Janzen, Spin trapping, Acc. Chem. Res. 4 (1971) 31–40, https://doi.org/10.1021/ar50037a005.

[63] M.J. Perkins, Spin trapping, in: V. Gold, D. Bethell (Eds.), Adv. Phys. Org. Chem., vol. 17, Academic Press, 1980, pp. 1–64, https://doi.org/10.1016/S0065-3160(08)60127-6.

[64] K.T. Knecht, R.P. Mason, In vivo spin trapping of xenobiotic free radical metabolites, Arch. Biochem. Biophys. 303 (1993) 185–194, https://doi.org/10.1006/abbi.1993.1272.

[65] M.J.D. Davies, G.S. Timmins, R.J.H. Clark, R.E. Hester, EPR Spectroscopy of Biologically Relevant Free Radicals in Cellular, Ex Vivo, and in Vivo Systems. Biomed. Appl. Spectrosc., John Wiley & Sons Ltd, 1996, pp. 217–266.

[66] D.R. Truzzi, O. Augusto, P.C. Ford, Thiyl radicals are co-products of dinitrosyl iron complex (DNIC) formation, Chem. Commun. 55 (2019) 9156–9159, https://doi.org/10.1039/C9CC04454J.

[67] M.J. Davies, Detection and identification of macromolecule-derived radicals by EPR spin trapping, Res. Chem. Intermed. 19 (1993) 669–679, https://doi.org/10.1163/156856793X00307.

[68] M.J. Davies, C.L. Hawkins, EPR Spin trapping of protein radicals, Free Radic. Biol. Med. 36 (2004) 1072–1086, https://doi.org/10.1016/j.freeradbiomed.2003.12.013.

[69] E.G. Janzen, J.L. Poyer, C.F. Schaefer, P.E. Downs, C.M. DuBose, Biological spin trapping II. Toxicity of nitrone spin traps: dose-ranging in the rat, J. Biochem. Biophys. Methods 30 (1995) 239–247, https://doi.org/10.1016/0165-022X(95)00012-1.

[70] R.F. Haseloff, K. Mertsch, E. Rohde, I. Baeger, I.A. Grigor'ev, I.E. Blasig, Cytotoxicity of spin trapping compounds, FEBS Lett. 418 (1997) 73–75, https://doi.org/10.1016/S0014-5793(97)01349-5.

[71] M.J. Burkitt, R.P. Mason, Direct evidence for in vivo hydroxyl-radical generation in experimental iron overload: an ESR spin-trapping investigation, Proc. Natl. Acad. Sci. USA 88 (1991) 8440–8444, https://doi.org/10.1073/pnas.88.19.8440.

[72] M. Sentjurk, R.P. Mason, Inhibition of radical adduct reduction and reoxidation of the corresponding hydroxylamines in in vivo spin trapping of carbon tetrachloride-derived radicals, Free Radic. Biol. Med. 13 (1992) 151–160, https://doi.org/10.1016/0891-5849(92)90077-T.

[73] W. Chamulitrat, M.S. Cohen, R.P. Mason, Free radical formation from organic hydroperoxides in isolated human polymorphonuclear neutrophils, Free Radic. Biol. Med. 11 (1991) 439–445, https://doi.org/10.1016/0891-5849(91)90059-C.

[74] C. Frejaville, H. Karoui, B. Tuccio, F.L. Moigne, M. Culcasi, S. Pietri, et al., 5-(Diethoxyphosphoryl)-5-methyl-1-pyrroline N-oxide: a new efficient phosphorylated nitrone for the in vitro and in vivo spin trapping of oxygen-centered radicals, J. Med. Chem. 38 (1995) 258–265, https://doi.org/10.1021/jm00002a007.

[75] H. Shi, G. Timmins, M. Monske, A. Burdick, B. Kalyanaraman, Y. Liu, et al., Evaluation of spin trapping agents and trapping conditions for detection of cell-generated reactive oxygen species, Arch. Biochem. Biophys. 437 (2005) 59–68, https://doi.org/10.1016/j.abb.2005.02.028.

[76] H. Zhang, J. Joseph, C. Felix, B. Kalyanaraman, Bicarbonate enhances the hydroxylation, nitration, and peroxidation reactions catalyzed by copper, zinc superoxide dismutase. Intermediacy of carbonate anion radical, J. Biol. Chem. 275 (2000) 14038–14045.

[77] M.G. Bonini, S. Miyamoto, P. Di Mascio, O. Augusto, Production of the carbonate radical anion during xanthine oxidase turnover in the presence of bicarbonate, J. Biol. Chem. 279 (2004) 51836–51843, https://doi.org/10.1074/jbc.M406929200.

[78] N. Hogg, Detection of nitric oxide by electron paramagnetic resonance spectroscopy, Free Radic. Biol. Med. 49 (2010) 122–129, https://doi.org/10.1016/j.freeradbiomed.2010.03.009.

[79] E.S. Lima, M.G. Bonini, O. Augusto, H.V. Barbeiro, H.P. Souza, D.S.P. Abdalla, Nitrated lipids decompose to nitric oxide and lipid radicals and cause vasorelaxation, Free Radic. Biol. Med. 39 (2005) 532–539, https://doi.org/10.1016/j.freeradbiomed.2005.04.005.

[80] M.N. Möller, N. Rios, M. Trujillo, R. Radi, A. Denicola, B. Alvarez, Detection and quantification of nitric oxide-derived oxidants in biological systems, J. Biol. Chem. 294 (2019) 14776–14802, https://doi.org/10.1074/jbc.REV119.006136.

[81] S.M. Vaz, F.M. Prado, P. Di Mascio, O. Augusto, Oxidation and nitration of ribonuclease and lysozyme by peroxynitrite and myeloperoxidase, Arch. Biochem. Biophys. 484 (2009) 127–133, https://doi.org/10.1016/j.abb.2008.12.017.

[82] P.K. Witting, A.G. Mauk, Reaction of Human Myoglobin and H2O2: electron transfer between tryrosine 103 phenoxyl radical and cysteine 110 yields a protein-tyil radical, J. Biol. Chem. 276 (2001) 16540–16547, https://doi.org/10.1074/jbc.M011707200.

[83] O. Augusto, S. Lopes de Menezes, E. Linares, N. Romero, R. Radi, A. Denicola, EPR detection of glutathiyl and hemoglobin-cysteinyl radicals during the interaction of peroxynitrite with human erythrocytes, Biochemistry 41 (2002) 14323–14328, https://doi.org/10.1021/bi0262202.

[84] L.J. Deterding, D.C. Ramirez, J.R. Dubin, R.P. Mason, K.B. Tomer, Identification of free radicals on hemoglobin from its self-peroxidation using mass spectrometry and ommuno-spin trapping: observation of a histidinyl radical, J. Biol. Chem. 279 (2004) 11600–11607, https://doi.org/10.1074/jbc.M310704200.

[85] C.E. Weller, A. Dhall, F. Ding, E. Linares, S.D. Whedon, N.A. Senger, et al., Aromatic thiol-mediated cleavage of N-O bonds enables chemical ubiquitylation of folded proteins, Nat. Commun. 7 (2016), 12979, https://doi.org/10.1038/ncomms12979.

[86] L.S. Nakao, M.B. Kadiiska, R.P. Mason, M.T. Grijalba, O. Augusto, Metabolism of acetaldehyde to methyl and acetyl radicals: in vitro and in vivo electron paramagnetic resonance spin-trapping studies, Free Radic. Biol. Med. 29 (2000) 721–729, https://doi.org/10.1016/s0891-5849(00)00374-9.

[87] R.P. Mason, Using anti-5,5-dimethyl-1-pyrroline N-oxide (anti-DMPO) to detect protein radicals in time and space with immuno-spin trapping, Free Radic. Biol. Med. 36 (2004) 1214–1223, https://doi.org/10.1016/j.freeradbiomed.2004.02.077.

[88] R.P. Mason, Imaging free radicals in organelles, cells, tissue, and in vivo with immuno-spin trapping, Redox Biol. 8 (2016) 422–429, https://doi.org/10.1016/j.redox.2016.04.003.

[89] R.A. Towner, N. Smith, D. Saunders, M. Henderson, K. Downum, F. Lupu, et al., In vivo imaging of immuno-spin trapped radicals with molecular magnetic resonance imaging in a diabetic mouse model, Diabetes 61 (2012) 2405–2413, https://doi.org/10.2337/db11-1540.

[90] R.A. Towner, N. Smith, D. Saunders, F. Lupu, R. Silasi-Mansat, M. West, et al., In vivo detection of free radicals using molecular MRI and immuno-spin trapping in a mouse model for amyotrophic lateral sclerosis, Free Radic. Biol. Med. 63 (2013) 351–360, https://doi.org/10.1016/j.freeradbiomed.2013.05.026.

[91] G.R. Buettner, L.W. Oberley, Considerations in the spin trapping of superoxide and hydroxyl radical in aqueous systems using 5,5-dimethyl-1-pyrroline-1-oxide, Biochem. Biophys. Res. Commun. 83 (1978) 69–74, https://doi.org/10.1016/0006-291X(78)90398-4.

[92] L. Hamilton, B.R. Nielsen, C.A. Davies, M.C.R. Symons, P.G. Winyard, Purity of different preparations of sodium 3,5-dibromo-4-nitrosobenzenesulphonate and their applicability for EPR spin trapping, Free Radic. Res. 37 (2003) 41–49, https://doi.org/10.1080/1071576021000028451.

[93] H.M. Swartz, M. Sentjurc, P.D. Morse, Cellular metabolism of water-soluble nitroxides: effect on rate of reduction of cell/nitroxide ratio, oxygen concentrations and permeability of nitroxides, Biochim Biophys Acta BBA - Mol Cell Res 888 (1986) 82–90, https://doi.org/10.1016/0167-4889(86)90073-X.

[94] B. Fink, S. Dikalov, E. Bassenge, A new approach for extracellular spin trapping of nitroglycerin-induced superoxide radicals both in vitro and in vivo, Free Radic. Biol. Med. 28 (2000) 121–128, https://doi.org/10.1016/S0891-5849(99)00228-2.

[95] S. Dikalov, M. Skatchkov, B. Fink, E. Bassenge, Quantification of superoxide radicals and peroxynitrite in vascular cells using oxidation of sterically hindered hydroxylamines and electron spin resonance, Nitric Oxide 1 (1997) 423–431, https://doi.org/10.1006/niox.1997.0139.

[96] S. Dikalov, M. Skatchkov, E. Bassenge, Spin trapping of superoxide radicals and peroxynitrite by 1-hydroxy-3-carboxy-pyrrolidine and 1-hydroxy-2,2,6,6-tetra-methyl-4-oxo-piperidine and the stability of corresponding nitroxyl radicals towards biological reductants, Biochem. Biophys. Res. Commun. 231 (1997) 701–704, https://doi.org/10.1006/bbrc.1997.6174.

[97] W.R. Hagen, EPR spectroscopy as a probe of metal centres in biological systems, Dalton Trans Camb Engl (2003 2006) 4415, https://doi.org/10.1039/b608163k. –34.

[98] S. Ye, Probing electronic structures of transition metal complexes using electron paramagnetic resonance spectroscopy, Magn. Reson Lett. 3 (2023) 43–60, https://doi.org/10.1016/j.mrl.2022.06.002.
[99] J.R. Stone, R.H. Sands, W.R. Dunham, M.A. Marletta, Spectral and ligand-binding properties of an unusual hemoprotein, the ferric form of soluble guanylate cyclase, Biochemistry 35 (1996) 3258–3262, https://doi.org/10.1021/bi952386+.
[100] J.R. Stone, R.H. Sands, W.R. Dunham, M.A. Marletta, Electron Paramagnetic Resonance spectral evidence for the formation of a pentacoordinate nitrosyl-heme complex on soluble guanylate cyclase, Biochem. Biophys. Res. Commun. 207 (1995) 572–577, https://doi.org/10.1006/bbrc.1995.1226.
[101] F.A. Taiwo, Electron paramagnetic resonance spectroscopic studies of iron and copper proteins, J. Spectrosc. 17 (2003) 53–63, https://doi.org/10.1155/2003/673567.
[102] J.P. Renault, C. Verchère-Béaur, I. Morgenstern-Badarau, F. Yamakura, M. Gerloch, EPR and ligand field studies of iron superoxide dismutases and iron-substituted manganese superoxide dismutases: relationships between electronic structure of the active site and activity, Inorg. Chem. 39 (2000) 2666–2675, https://doi.org/10.1021/ic0000451.
[103] G. Rotilio, L. Morpurgo, C. Giovagnoli, L. Calabrese, B. Mondovi, Metal sites of copper proteins. III. Symmetry of copper in bovine superoxide dismutase and its functional significance, Biochemistry 11 (1972) 2187–2192, https://doi.org/10.1021/bi00761a028.
[104] P. Geijer, S. Peterson, K.A. Åhrling, Z. Deák, S. Styring, Comparative studies of the S0 and S2 multiline electron paramagnetic resonance signals from the manganese cluster in Photosystem II, Biochim. Biophys. Acta BBA - Bioenerg. 1503 (2001) 83–95, https://doi.org/10.1016/S0005-2728(00)00224-3.
[105] M. Xia, R. Dempski, R. Hille, The reductive half-reaction of xanthine oxidase: reaction with aldehyde substrates and identification of the catalytically labile oxygen, J. Biol. Chem. 274 (1999) 3323–3330, https://doi.org/10.1074/jbc.274.6.3323.
[106] G. Rao, R.D. Britt, Electronic structure of two catalytic states of the [FeFe] hydrogenase H-cluster as probed by pulse electron paramagnetic resonance spectroscopy, Inorg. Chem. 57 (2018) 10935–10944, https://doi.org/10.1021/acs.inorgchem.8b01557.
[107] C.R. Fontenot, H. Tasnim, K.A. Valdes, C.V. Popescu, H. Ding, Ferric uptake regulator (Fur) reversibly binds a [2Fe-2S] cluster to sense intracellular iron homeostasis in Escherichia coli, J. Biol. Chem. 295 (2020) 15454–15463, https://doi.org/10.1074/jbc.RA120.014814.
[108] M.-R. Wu, L.-L. Miao, Y. Liu, X.-X. Qian, T.-T. Hou, G.-M. Ai, et al., Identification and characterization of a novel hydroxylamine oxidase, DnfA, that catalyzes the oxidation of hydroxylamine to N2, J. Biol. Chem. 298 (2022), 102372, https://doi.org/10.1016/j.jbc.2022.102372.
[109] A.F. Vanin, Dinitrosyl iron complexes with thiolate ligands: physico-chemistry, biochemistry and physiology, Nitric Oxide-Biol Chem 21 (2009) 1–13, https://doi.org/10.1016/j.niox.2009.03.005.
[110] E. Linares, L.S. Nakao, O. Augusto, M.B. Kadiiska, EPR studies of in vivo radical production by lipopolysaccharide: potential role of iron mobilized from iron-nitrosyl complexes, Free Radic. Biol. Med. 34 (2003) 766–773, https://doi.org/10.1016/s0891-5849(02)01424-7.
[111] N. Lehnert, E. Kim, H.T. Dong, J.B. Harland, A.P. Hunt, E.C. Manickas, et al., The biologically relevant coordination chemistry of iron and nitric oxide: electronic structure and reactivity, Chem. Rev. 121 (2021) 14682–14905, https://doi.org/10.1021/acs.chemrev.1c00253.
[112] H. Lewandowska, M. Kalinowska, K. Brzóska, K. Wójciuk, G. Wójciuk, M. Kruszewski, Nitrosyl iron complexes-synthesis, structure and biology, Dalton Trans. 40 (2011) 8273–8289, https://doi.org/10.1039/C0DT01244K.
[113] J.R. Lancaster, J.B. Hibbs, EPR demonstration of iron-nitrosyl complex formation by cytotoxic activated macrophages, Proc. Natl. Acad. Sci. U. S. A. 87 (1990) 1223–1227, https://doi.org/10.1073/pnas.87.3.1223.
[114] J. Stadler, H.A. Bergonia, M. Di Silvio, M.A. Sweetland, T.R. Billiar, R.L. Simmons, et al., Nonheme iron-nitrosyl complex formation in rat hepatocytes: detection by electron paramagnetic resonance spectroscopy, Arch. Biochem. Biophys. 302 (1993) 4–11, https://doi.org/10.1006/abbi.1993.1173.
[115] T.-T. Lu, Y.-M. Wang, C.-H. Hung, S.-J. Chiou, W.-F. Liaw, Bioinorganic xhemistry of the natural [Fe(NO)2] motif: evolution of a functional model for NO-related biomedical application and revolutionary development of a translational model, Inorg. Chem. 57 (2018) 12425–12443, https://doi.org/10.1021/acs.inorgchem.8b01818.
[116] D.R. Truzzi, N.M. Medeiros, O. Augusto, P.C. Ford, Dinitrosyl iron complexes (DNICs). from spontaneous assembly to biological roles, Inorg. Chem. 60 (2021) 15835–15845, https://doi.org/10.1021/acs.inorgchem.1c00823.
[117] D.R. Truzzi, O. Augusto, A.V. Iretskii, P.C. Ford, Dynamics of dinitrosyl iron complex (DNIC) formation with low molecular weight thiols, Inorg. Chem. 58 (2019) 13446–13456, https://doi.org/10.1021/acs.inorgchem.9b02338.
[118] D.R. Truzzi, S.V. Alves, L.E.S. Netto, O. Augusto, The peroxidatic thiol of peroxiredoxin 1 is nitrosated by nitrosoglutathione but coordinates to the dinitrosyl iron complex of glutathione, Antioxidants 9 (2020) 276, https://doi.org/10.3390/antiox9040276.
[119] H.C. Lok, S. Sahni, V. Richardson, D.S. Kalinowski, Z. Kovacevic, D.J.R. Lane, et al., Glutathione S-transferase and MRP1 form an integrated system involved in the storage and transport of dinitrosyl–dithiolato iron complexes in cells, Free Radic. Biol. Med. 75 (2014) 14–29, https://doi.org/10.1016/j.freeradbiomed.2014.07.002.
[120] Z. Kovacevic, S. Sahni, H. Lok, M.J. Davies, D.A. Wink, D.R. Richardson, Regulation and control of nitric oxide (NO) in macrophages: protecting the "professional killer cell" from its own cytotoxic arsenal via MRP1 and GSTP1, Biochim. Biophys. Acta Gen. Subj. 1861 (2017) 995–999, https://doi.org/10.1016/j.bbagen.2017.02.021.
[121] M. Boese, P. Mordvintcev, A. Vanin, R. Busse, A. Mulsch, S-nitrosation of serum-albumin by dinitrosyl-iron complex, J. Biol. Chem. 270 (1995) 29244–29249, https://doi.org/10.1074/jbc.270.49.29244.
[122] C.A. Bosworth, J.C. Toledo, J.W. Zmijewski, Q. Li, J.R. Lancaster, Dinitrosyliron complexes and the mechanism(s) of cellular protein nitrosothiol formation from nitric oxide, Proc. Natl. Acad. Sci. U. S. A. 106 (2009) 4671–4676, https://doi.org/10.1073/pnas.0710416106.
[123] A.L. Kleschyov, P. Wenzel, T. Munzel, Electron paramagnetic resonance (EPR) spin trapping of biological nitric oxide, Anal -ArginineNO Pathw 851 (2007) 12–20, https://doi.org/10.1016/j.jchromb.2006.10.006.
[124] L.V. Modolo, O. Augusto, I.M.G. Almeida, J.R. Magalhaes, I. Salgado, Nitrite as the major source of nitric oxide production by Arabidopsis thaliana in response to Pseudomonas syringae, FEBS Lett. 579 (2005) 3814–3820, https://doi.org/10.1016/j.febslet.2005.05.078.
[125] R. Ahmad, P. Kuppusamy, Theory, instrumentation, and applications of electron paramagnetic resonance oximetry, Chem. Rev. 110 (2010) 3212–3236, https://doi.org/10.1021/cr900396q.
[126] P. Kuppusamy, Sense and sensibility of oxygen in pathophysiology using EPR oximetry, in: L.J. Berliner, N.L. Parinandi (Eds.), Meas. Oxid. Oxidative Stress Biol. Syst., vol. 34, Springer International Publishing, Cham, 2020, pp. 135–187, https://doi.org/10.1007/978-3-030-47318-1_9.
[127] W.L. Hubbell, C. Altenbach, Investigation of structure and dynamics in membrane proteins using site-directed spin labeling, Curr. Opin. Struct. Biol. 4 (1994) 566–573, https://doi.org/10.1016/S0959-440X(94)90219-4.
[128] W.L. Hubbell, C.J. López, C. Altenbach, Z. Yang, Technological advances in site-directed spin labeling of proteins, Protein-Carbohydr. Interact Biophys. Method 23 (2013) 725–733, https://doi.org/10.1016/j.sbi.2013.06.008.
[129] W.K. Subczynski, J.S. Hide, A. Kusumi, Oxygen permeability of phosphatidylcholine-cholesterol membranes, Proc. Natl. Acad. Sci. USA 86 (1989) 4474–4478.
[130] A. Ligeza, A.N. Tikhonov, J.S. Hyde, W.K. Subczynski, Oxygen permeability of thylakoid membranes: electron paramagnetic resonance spin labeling study, Biochim. Biophys. Acta BBA - Bioenerg. 1365 (1998) 453–463, https://doi.org/10.1016/S0005-2728(98)00098-X.
[131] J. Widomska, M. Raguz, W.K. Subczynski, Oxygen permeability of the lipid bilayer membrane made of calf lens lipids, Biochim Biophys Acta BBA - Biomembr 1768 (2007) 2635–2645, https://doi.org/10.1016/j.bbamem.2007.06.018.
[132] M. Takahashi, J. Tsuchiya, E. Niki, Scavenging of radicals by vitamin E in the membranes as studied by spin labeling, J. Am. Chem. Soc. 111 (1989) 6350–6353, https://doi.org/10.1021/ja00198a054.
[133] S.P. Gabbita, D.A. Butterfield, K. Hensley, W. Shaw, J.M. Carney, Aging and caloric restriction affect mitochondrial respiration and lipid membrane status: an electron paramagnetic resonance investigation, Free Radic. Biol. Med. 23 (1997) 191–201, https://doi.org/10.1016/S0891-5849(97)00043-9.
[134] K. Tsuda, K. Kimura, I. Nishio, Y. Masuyama, Nitric oxide improves membrane fluidity of erythrocytes in essential hypertension: an electron paramagnetic resonance investigation, Biochem. Biophys. Res. Commun. 275 (2000) 946–954, https://doi.org/10.1006/bbrc.2000.3408.